$Tl_2Ch_2^{2-}$ (Ch = Se and/or Te) Anions: X-ray Crystal Structures and Raman Spectra of (2,2,2-crypt-K^+)$_2Tl_2Se_2^{2-}$ and (2,2,2-crypt-K^+)$_2Tl_2Te_2^{2-}$ and Solution ^{77}Se, ^{203}Tl, and ^{205}Tl NMR Spectroscopic and Theoretical Studies of $Tl_2Ch_2^{2-}$, $In_2Se_2^{2-}$, and $In_2Te_2^{2-}$ †

Horst Borrmann,[1] Janette Campbell,[2] David A. Dixon,[3] Hélène P. A. Mercier,[2] Ayaaz M. Pirani,[2] and Gary J. Schrobilgen*,[2]

Max-Planck-Institut für Festkörperforschung, Heisenbergstrasse 1, Stuttgart D-70569, Germany, Department of Chemistry, McMaster University, Hamilton, Ontario L8S 4M1, Canada, and William R. Wiley Environmental Molecular Sciences Laboratory, Pacific Northwest National Laboratory, 906 Battelle Blvd., P.O. Box 999, KI-83 Richland, Washington 99352

Received August 19, 1997

The seleno- and tellurothallate(I) anions $Tl_2Ch_2^{2-}$ (Ch = Se and/or Te) and the ^{77}Se-enriched $Tl_2Se_2^{2-}$ anion have been obtained by extraction of the alloys MTlCh (M = Na, K; Ch = Se, Te), $KTlSe_{0.5}Te_{0.5}$, and ^{77}Se-enriched KTlSe in ethylenediamine and liquid NH_3 and in the presence of a stoichiometric excess of 2,2,2-crypt with respect to M^+. The butterfly-shaped $Tl_2Ch_2^{2-}$ anions were characterized in solution by ^{77}Se, ^{203}Tl, and ^{205}Tl NMR spectroscopy, Raman spectroscopy, and X-ray crystallography in (2,2,2-crypt-K^+)$_2Tl_2Ch_2^{2-}$. The energy-minimized structures of the $Tl_2Ch_2^{2-}$ (Ch = Se and/or Te) anions were calculated by using density functional theory calculations confirming the nonplanar geometries of all three anions, which are compared with those of the presently unknown $In_2Ch_2^{2-}$ (Ch = Se, Te) anions. The magnitudes of the relativistically corrected reduced coupling constants, $(K_{Tl-Ch})_{RC}$, are consistent with essentially pure p-bonded rings whereas the magnitudes of $(K_{Tl-Tl})_{RC}$ suggest significant s electron density along the Tl···Tl axes and is confirmed by theory. Density functional theory calculations were also used to assign the solid-state vibrational spectra of $Tl_2Se_2^{2-}$ and $Tl_2Te_2^{2-}$. The variation of the ^{205}Tl−^{203}Tl spin−spin coupling constants with solvent and temperature, the differences between the calculated and experimentally determined fold angles, and the low experimental and calculated vibrational frequencies of the anion deformation modes indicate that the anion geometries are significantly influenced by environmental factors.

Introduction

It has been recognized for some time that many Zintl type anions are analogous to better known compounds formed by the elements from the first and second rows of the periodic table.[4] For example, the homopolyatomic E_5^{2-} (E = Ge,[5] Sn,[6] Pb[6]) clusters possess skeletal bonding arrangements similar to those exhibited by $B_5H_5^{2-}$ and $C_2B_3H_5$,[4,7] and the square-planar 6π-electron quasi-aromatic Sb_4^{2-} [8] and Bi_4^{2-} [9] anions with 22 valence electrons possess bonding arrangements similar to those of P_4^{2-} [10] and $C_4H_4^{2-}$.[4] The 20 valence electron Pb_4^{4-},[11] Tl_4^{8-},[12] $Sn_2Bi_2^{2-}$,[13] and $Pb_2Sb_2^{2-}$ [14] anions exhibit tetrahedral geometries that are isovalent with P_4,[15] As_4,[16] and Sb_4[16] and are consistent with localized valence structures having covalent 2-center−2-electron bonds directed along the six edges of the tetrahedron and one valence lone electron pair on each atom.[17] The bonding molecular orbitals have been shown to consist of a combination of essentially pure p-orbitals, whereas the lone-electron pair molecular orbitals consist of valence s-orbitals.[17,18] The HOMO's were shown to be composed primarily of p-orbitals on the electropositive atoms, and the LUMO's, which possess antibonding character, were shown to be localized primarily on the more electronegative atoms. Interestingly, the $Tl_2Te_2^{2-}$ anion,[19] which is isovalent with $Sn_2Bi_2^{2-}$, $Pb_2Sb_2^{2-}$, and P_4, exhibits a unique butterfly geometry in which the thallium atoms lie along the fold of the wings and is intermediate between the tetrahedral geometry adapted by 20-valence-electron systems and the square-planar geometry associated with tetranuclear species having 22 valence electrons. The departure from the tetrahedral geometry has been attributed to the large separation of the Tl and Te atoms in the periodic table.[17,18] A purely ionic model describing the bonding in $Tl_2Te_2^{2-}$ as the coordination of two Tl^+ cations and two Te^{2-} anions has therefore been proposed.[17] In contrast, a covalent model, as in P_4, has been

† Dedicated to the memory of Professor Alfio Corsini (April 28, 1934−December 4, 1997).

(1) Max-Planck-Institut.
(2) McMaster University.
(3) Pacific Northwest National Laboratory.
(4) Corbett, J. D. *Chem. Rev.* **1985**, *85*, 383.
(5) Campbell, J.; Schrobilgen, G. J. *Inorg. Chem.* **1997**, *36*, 4078.
(6) Edwards, P. A.; Corbett, J. D. *Inorg. Chem.* **1977**, *16*, 903.
(7) Corbett, J. D. *Inorg. Chem.* **1968**, *7*, 198.
(8) Critchlow, S. C.; Corbett, J. D. *Inorg. Chem.* **1984**, *23*, 770.
(9) Cisar, A.; Corbett, J. D. *Inorg. Chem.* **1977**, *16*, 2482.
(10) Martin, T. P. *Angew. Chem., Int. Ed. Engl.* **1986**, *25*, 197.
(11) Marsh, R. E.; Shoemaker, D. P. *Acta Crystallogr.* **1953**, *6*, 197.
(12) Hansen, D. A.; Smith, J. F. *Acta Crystallogr.* **1967**, *22*, 836.
(13) Critchlow, S. C.; Corbett, J. D. *Inorg. Chem.* **1982**, *21*, 3286.
(14) Critchlow, S. C.; Corbett, J. D. *Inorg. Chem.* **1985**, *24*, 979
(15) Simon, A.; Borrmann, H.; Craubner, H. *Phosphorus Sulfur* **1987**, *30*, 507.
(16) Donohue, J. *The Structures of the Elements*; John Wiley & Sons, Inc.: New York, 1974; Chapter 8, pp 302−310.
(17) Marynick, D. S.; Axe, F. U. *Inorg. Chem.* **1988**, *27*, 1426.
(18) Cave, R. J.; Davidson, E. R.; Sautet, P.; Canadell, E.; Eisenstein, O. *J. Am. Chem. Soc.* **1989**, *111*, 8105.
(19) Burns, R. C.; Corbett, J. D. *J. Am. Chem. Soc.* **1981**, *103*, 2627.

S0020-1669(97)01046-X CCC: $15.00
Published on Web 04/01/1998

used to describe the bonding in $Sn_2Bi_2^{2-}$ and $Pb_2Sb_2^{2-}$ which contain atoms that are closer to one another in the periodic table.[17] The puckering observed for the $Tl_2Te_2^{2-}$ anion in (2,2,2-crypt-K^+)$_2Tl_2Te_2^{2-}$·en[19] is, however, inconsistent with a purely ionic model because the arrangement of ions in ionic compounds tends to minimize Coulombic repulsions by maximizing interatomic distances and would be expected to give a planar structure for $(Tl^+)_2(Te^{2-})_2$. The distortion from planarity has been attributed, using spin-restricted scattered-wave Xα calculations,[17] to the repulsive interaction between the antisymmetric combination of the Tl 6s atomic orbitals and the occupied molecular orbital composed primary of Te 5p atomic orbitals. *Ab initio* and extended Hückel calculations on tetranuclear 20-electron systems[18] have indicated that an energetic interchange of the frontier molecular orbitals associated with a greater electronegativity difference between the bonding atoms can account for the preference of the butterfly geometry adopted by $Tl_2Te_2^{2-}$ over the tetrahedral one. *Ab initio* and extended Hückel calculations predict a planar structure for the isoelectronic 20 valence-electron system, Tl_2I_2, in which the electronegativity difference between the atoms is larger when compared to that in the $Tl_2Te_2^{2-}$ anion. Accordingly, a more planar structure is anticipated for the crystallographically uncharacterized $Tl_2Se_2^{2-}$ anion when compared to the Te analog.

Although the $Tl_2Ch_2^{2-}$ (Ch = Se and/or Te) anions have been characterized by solution multi-NMR spectroscopy[20] and the $Tl_2Te_2^{2-}$ anion has been characterized by X-ray crystallography in (2,2,2-crypt-K^+)$_2Tl_2Te_2^{2-}$·en,[19] the X-ray crystal structure of $Tl_2Se_2^{2-}$ has never been reported, nor have the vibrational spectra of these anions been published. The $Tl_2Ch_2^{2-}$ anion vibrational modes, including that associated with the inversion mode of the anions along the fold angle (the dihedral angle between the two Tl_2Ch planes in the anion structures), are anticipated to be extremely low in energy. The anticipated deformability of the $Tl_2Ch_2^{2-}$ anions about the fold angle may be strongly influenced by environmental factors such as crystal packing and solvent coordination and may give rise to energy-minimized geometries in the gas phase having Tl···Tl distances and fold angles significantly different than those in the solid state. Only single-point theoretical calculations have been reported[17,18] for the experimental $Tl_2Te_2^{2-}$ anion geometry in (2,2,2-crypt-K^+)$_2Tl_2Te_2^{2-}$·en,[19] and no attempts have been made to optimize the gas-phase geometry of the anion. A comparison of the gas-phase geometry with the experimental one should provide a means to assess the extent to which environmental factors influence the geometries of the $Tl_2Ch_2^{2-}$ anions.

The present paper reports a more detailed variable-temperature solution multi-NMR spectroscopic characterization of the $Tl_2Ch_2^{2-}$ (Ch = Se and/or Te) anions in ethylenediamine (en) and/or liquid ammonia solvents and the X-ray crystal structures of the $Tl_2Ch_2^{2-}$ (Ch = Se or Te) anions in the (2,2,2-crypt-K^+)$_2Tl_2Ch_2^{2-}$ salts, where the structure of $Tl_2Se_2^{2-}$ is reported for the first time and that of $Tl_2Te_2^{2-}$ is reported in the absence of solvent in the crystal lattice. Density functional theory (DFT) calculations at the local (LDFT) and nonlocal (NLDFT) levels have been used to derive the energy-minimized geometries of the $Tl_2Ch_2^{2-}$ (Ch = Se and/or Te) anions and to study the nature of the bonding in these anions. Vibrational frequencies derived from DFT calculations have also been used to assign the experimental vibrational spectra of the $Tl_2Ch_2^{2-}$ anions.

(20) Burns, R. C.; Devereux, L. A.; Granger, P.; Schrobilgen, G. J. *Inorg. Chem.* **1985**, *24*, 2615.

Table 1. Summary of Crystal Data and Refinement Results for (2,2,2-crypt-K^+)$_2Tl_2Ch_2^{2-}$ (Ch = Se and Te)

	(2,2,2-crypt-K^+)$_2Tl_2Se_2^{2-}$	(2,2,2-crypt-K^+)$_2Tl_2Te_2^{2-}$
formula	$C_{36}H_{72}K_2N_4O_{12}Se_2Tl_2$	$C_{36}H_{72}K_2N_4O_{12}Te_2Tl_2$
fw	1397.84	1495.12
space group	$P2_1/m$ (No. 11)	$P\bar{1}$ (No. 2)
a (Å)	11.526(4)	10.976(2)
b (Å)	10.470(3)	11.112(2)
c (Å)	21.623(7)	11.629(2)
α (deg)	90.00	64.05(3)
β (deg)	91.90(3)	84.29(3)
γ (deg)	90.00	81.47(3)
V (Å^3)	2608.0(14)	1260.3(4)
Z	2	1
T (°C)	24	−123
λ (Å)	0.560 86	0.710 73
ρ_{calcd} (g cm^{-3})	1.780	1.970
μ (cm^{-1})	42.24	77.40
R_1[a]	0.0936	0.0743
wR_2[b]	0.2826	0.1930

[a] $R_1 = (\sum||F_o| - |F_c||)/\sum|F_o|$ for $I > 2\sigma(I)$. [b] w$R_2 = [\sum[w(F_o^2 - F_c^2)^2]/\sum w(F_o^2)^2]^{1/2}$ for $I > 2\sigma(I)$.

Table 2. Atomic Coordinates ($\times 10^4$) and Equivalent Isotropic Displacement Coefficients (Å$^2 \times 10^3$) for the $Tl_2Ch_2^{2-}$ Anions in (2,2,2-crypt-K^+)$_2Tl_2Ch_2^{2-}$ (Ch = Se and Te)

		x	y	z	U_{eq}[a]
$Tl_2Se_2^{2-}$	Tl(1)	2324(1)	734(1)	7438(1)	62(1)
	Se(1)	4122(3)	2500	7544(2)	53(1)
	Se(2)	527(3)	2500	7492(2)	56(1)
$Tl_2Te_2^{2-}$	Tl(1a)	3428(3)	9985(3)	4459(2)	40(1)
	Tl(1b)	3605(3)	9774(3)	4269(2)	40(1)
	Te(1a)	4817(4)	7880(6)	6639(4)	44(1)
	Te(1b)	5070(3)	7843(6)	6471(4)	44(1)

[a] Equivalent isotropic U is defined as one-third of the trace of the othogonalized $\mathbf{U}_{ij}$ tensor.

Results and Discussion

Synthesis of the $Tl_2Ch_2^{2-}$ (Ch = Se and/or Te) Anions. The experimental approach involved the synthesis of the ternary MTlCh (M = Na, K; Ch = Se, Te), quaternary $KTlSe_{0.5}Te_{0.5}$, and ^{77}Se-enriched KTlSe (hereafter referred to as KTl^{77}Se) alloys by fusion of the elements followed by extraction of the powdered alloys in en or liquid NH_3 in the presence of a molar excess of 2,2,2-crypt with respect to M^+. Crystals of (2,2,2-crypt-K^+)$_2Tl_2Se_2^{2-}$ were obtained upon addition of THF to an en solution of KTlSe containing a molar excess of 2,2,2-crypt with respect to K^+. All attempts to obtain crystals of (2,2,2-crypt-K^+)$_2Tl_2Te_2^{2-}$ from an en solution of NaTlTe containing a molar excess of 2,2,2-crypt with respect to Na^+ resulted in the formation of microcrystalline material. Crystals of (2,2,2-crypt-K^+)$_2Tl_2Te_2^{2-}$ suitable for an X-ray structure determination were obtained upon addition of THF to a dark green en/ethylamine (1:1 v/v) solution resulting from the reaction of K_2Te and Tl_2Te in a 1:2 molar ratio in the presence of a 37 mol % deficit of 2,2,2-crypt with respect to K^+. The dark green solution was shown by ^{203,205}Tl NMR spectroscopy to contain the $Tl_2Te_2^{2-}$ anion as the major species in solution along with small amounts of $TlTe_3^{3-}$.

X-ray Crystal Structures of (2,2,2-crypt-K^+)$_2Tl_2Ch_2^{2-}$ (Ch = Se, Te). A summary of the refinement results and other crystallographic information is given in Table 1. The final atomic coordinates and equivalent isotropic thermal parameters for the $Tl_2Ch_2^{2-}$ (Ch = Se or Te) anions are summarized in Table 2, and those corresponding to the 2,2,2-crypt-K^+ cations are provided in the Supporting Information, Table S2. The most significant interatomic and transannular distances and the most

Table 3. Experimental and Calculated Geometries for the $Tl_2Ch_2^{2-}$ Anions (Ch = Se and/or Te)

		LDFT		NLDFT		
	exptl[b]	PP/PP	PP/DZVP	PP/PP	PP/DZVP	LDFT ECP
			$Tl_2Se_2^{2-}$ (C_{2v})			
Tl···Tl (Å)	3.698(2)	3.540	3.629	3.561	3.647	3.555
Tl−Se (Å)	2.781(3)	2.736	2.943	2.755	2.966	2.821
Se···Se (Å)	4.140(3)	3.993	4.555	4.024	4.587	4.219
Tl−Se−Tl (deg)	83.34(1)	80.6	76.1	80.5	75.9	78.1
Se−Tl−Se (deg)	96.21(7)	93.7	101.4	93.8	101.3	96.8
fold angle (deg)[a]	9.6	33.8	21.3	33.8	22.6	31.2
			$Tl_2Te_2^{2-}$ (C_{2v})			
Tl···Tl (Å)	3.798(2) [3.600(3)]	3.655	3.727	3.681	3.768	3.657
Tl−Te (Å)	2.956(2) [2.954(11)]	2.913	3.111	2.936	3.139	3.040
Te−Te (Å)	4.552(2) [4.414(3)]	4.302	4.813	4.337	4.851	4.690
Tl−Te−Tl (deg)	79.1(2) [75.1(3)]	77.7	73.6	77.7	73.8	74.0
Te−Tl−Te (deg)	97.7(2) [96.6(2)]	95.2	101.4	95.2	101.2	101.0
fold angle (deg)[a]	17.4 [39.9]	37.1	29.9	37.0	29.9	30.0

Tl_2SeTe^{2-} (C_s)

	LDFT PP/PP	NLDFT PP/PP	LDFT ECP/DZVP		LDFT PP/PP	NLDFT PP/PP	LDFT ECP/DZVP
Tl···Tl (Å)	3.583	3.612	3.600	Tl−Se−Tl (deg)	82.4	82.6	79.9
Tl−Se (Å)	2.720	2.735	2.802	Tl−Te−Tl (deg)	75.3	75.1	72.1
Tl−Te (Å)	2.934	2.962	3.060	Se−Tl−Te (deg)	94.5	94.9	98.8
Te−Se (Å)	4.155	4.198	4.455	fold angle (deg)[a]	38.7	35.1	31.0

[a] The fold angle in the $Tl_2Ch_2^{2-}$ (Ch = Se and/or Te) anion structures is the dihedral angle between the two Tl_2Ch planes. [b] Values reported in brackets refer to the $Tl_2Te_2^{2-}$ anion structure in (2,2,2-crypt-K^+)$_2Tl_2Te_2^{2-}$·en and are taken from ref 19. The fold angle reported for the $Tl_2Te_2^{2-}$ anion in ref 19, 49.9°, is a typographical error and should be 39.9°.

significant bond angles, including the fold angles, are listed in Table 3 along with the calculated values (see Computational Results).

The structure of the 2,2,2-crypt-K^+ cations in the title compounds is similar to that previously determined in K^+(2,2,2-crypt-K^+)$HOSnTe_3^{3-}$,[21] (2,2,2-crypt-K^+)$_4Pb_9^{4-}$,[22] and (2,2,2-crypt-K^+)$_2Tl_2Te_2^{2-}$·en,[19] with average K···O and K···N distances in the Se [Te] compound ranging from 2.77−2.87 [2.97−3.09] and 2.697(5)−2.791(5) [2.933(5)−2.955(6)] Å. A complete list of bond distances and angles in the 2,2,2-crypt-K^+ cations is provided in the Supporting Information, Table S3.

The crystal structure of the Se compound consists of ordered $Tl_2Se_2^{2-}$ anions and disordered 2,2,2-crypt-K^+ cations, whereas the structure of the Te analog consists of ordered 2,2,2-crypt-K^+ cations and $Tl_2Te_2^{2-}$ anions disordered about a center of symmetry. The most interesting aspect of the structures is the butterfly-shaped geometry of the anions (approximate C_{2v} point symmetry) in which the thallium atoms are located along the fold of the wings (Figure 1). This geometry has been previously observed in (2,2,2-crypt-K^+)$_2Tl_2Te_2^{2-}$·en.[19] The fold angle in $Tl_2Se_2^{2-}$ (9.6°) is significantly smaller than that in $Tl_2Te_2^{2-}$ (17.4°) and is consistent with the trend anticipated on the basis of VSEPR rules.[23] Interestingly, the fold angle in the present $Tl_2Te_2^{2-}$ anion is considerably smaller than in the previously characterized salt (39.9°)[19] and is discussed in a subsequent section (see Computational Results).

The Tl−Se distance in $Tl_2Se_2^{2-}$, 2.781(3) Å, is considerably shorter than the average Tl−Se distances observed in Tl($C_{12}N_{15}N_2OSe$) [3.112(4) Å][24] and in $Tl_2(Se_2C_2(CN)_2)_2^{2-}$ [3.143(4) Å].[25] The Tl−Te distance in $Tl_2Te_2^{2-}$ is 2.956(2) Å and is identical to the average bond distance [2.954(6) Å]

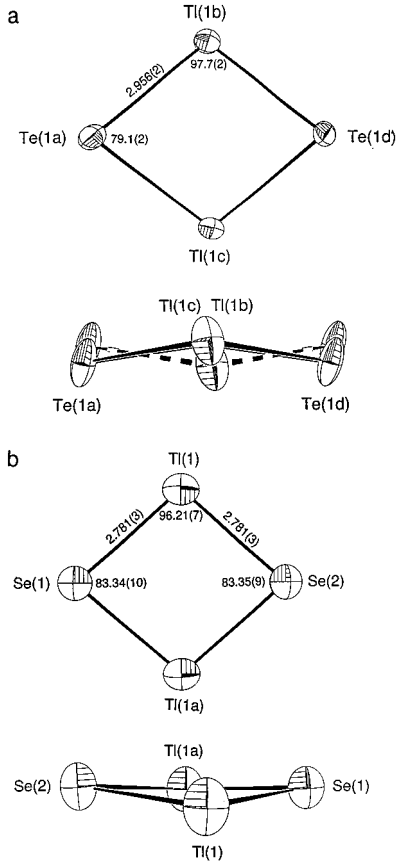

Figure 1. Views of the (a) $Tl_2Te_2^{2-}$ and (b) $Tl_2Se_2^{2-}$ anions in (2,2,2-crypt-K^+)$_2Tl_2Ch_2^{2-}$ (Ch = Se or Te) with displacement ellipsoids drawn at the 50% probability level.

observed in the previously characterized anion and is much shorter than those observed in the alloy phases TlTe [3.398(5)−3.648(3) Å][26] and Tl_5Te_3 [3.142(9)−3.596(4) Å].[26,27] The transannular Tl···Tl distances in $Tl_2Se_2^{2-}$ [3.698(2) Å] and in $Tl_2Te_2^{2-}$ [3.798(2) Å] are longer than in thallium metal (3.408

(21) Campbell, J.; Devereux, L. A.; Gerken, M.; Mercier, H. P. A.; Pirani, A. M.; Schrobilgen, G. J. *Inorg. Chem.* **1996**, *35*, 2945.
(22) Campbell, J.; Dixon, D. A.; Mercier, H. P. A.; Schrobilgen, G. J. *Inorg. Chem.* **1995**, *34*, 5798.
(23) Gillespie, R. J.; Hargittai, I. *The VSEPR Model of Molecular Geometry*; Simon & Schuster, Inc.: Boston, MA, 1991; Chapters 3 and 5.
(24) Bensch, W.; Schuster, M. *Z. Anorg. Allg. Chem.* **1993**, *619*, 1689.
(25) Zahn, G.; Franke, A.; Dietzsch, W. *Acta Crystallogr.* **1995**, *C51*, 854.

Table 4. Chemical Shifts and Spin−Spin Coupling Constants for $TlCh_3^{3-}$ and $Tl_2Ch_2^{2-}$ (Ch = Se, Te)

	chem shift, ppm		spin−spin coupling constants								
			J, Hz		*K*, $T^2\ J^{-1} \times 10^2$		K_{RC}, $T^2\ J^{-1} \times 10^{21}$				
anion	$^{203,205}Tl$	^{77}Se	$^{205}Tl-^{203}Tl$	$^{205}Tl-Ch^{a,b}$	Tl−Tl	Tl−Ch	Tl−Tl	Tl−Ch	solvent	*T*, °C	alloy
$TlSe_3^{3-}$	2804			7211		53.67		15.19	NH_3	−20	KTlSe
	2829	140		7250		53.96		15.27	NH_3	−60	KTlSe
	2844	136		7239		53.87		15.25	NH_3	−70	KTlSe
$Tl^{77}Se_3^{3-}$	2841	137		7227 (7159)		53.79		15.22	NH_3	−70	$KTl^{77}Se$
$Tl_2Se_2^{2-}$	7681		3995	2228	9.761	15.52	1.060	4.692	NH_3	−40	KTlSe
	7642	384	3791	2210	9.263	16.38	1.006	4.654	NH_3	−60	KTlSe
	7595	372	3602	2261 (2254)	8.801	16.76	0.9560	4.744	NH_3	−70	KTlSe
$Tl_2Se_2^{2-}$	7689		4506	2265	11.01	16.79	1.190	4.752	en	0	$KTlSe_{0.5}Te_{0.5}$
	7598		3661	2258 (2265)	8.945	16.74	0.9672	4.737	NH_3	−70	$KTlSe_{0.5}Te_{0.5}$
$Tl_2{}^{77}Se_2^{2-}$	7596	371	3560	2253 (2229)	8.698	16.70	0.9405	4.727	NH_3	−70	$KTl^{77}Se$
Tl_2SeTe^{2-}	7910		<2800		<6.8		<0.74		en	0	$KTlSe_{0.5}Te_{0.5}$
	7793		1945	2407 (Se)	4.752	17.84 (Se)	0.5138	5.050 (Se)	NH_3	−70	$KTlSe_{0.5}Te_{0.5}$
				3591 (Te)		16.02 (Te)		3.641 (Te)			
$TlTe_3^{3-}$	453			16371		73.05		16.60	en	0	NaTlTe
	426			16137 (13381)		72.00		16.36	NH_3	−70	KTlTe
$Tl_2Te_2^{2-}$	8175		6337	4004	15.48	17.87	1.674	4.060	en	0	NaTlTe
	8050		7591	3989	18.55	17.80	2.005	4.044	NH_3	-70	KTlTe
	8153		6328	4200	15.46	18.74	1.672	4.258	en/ethylamine	−20	K_2Te/Tl_2Te
	8128[c]		<200[c]	8006[c]	<0.50[c]	35.72[c]	<0.050[c]	8.115[c]	NH_3	−40	KTlTe

[a] Ch denotes ^{77}Se or ^{125}Te. [b] Values in parentheses denote $^1J(^{203}Tl-^{77}Se)$. [c] Values were obtained from ref 20.

Å)[28] but are considerably shorter than those observed in the $(C_6H_5)_4P^+$ [4.047(1)−4.381(1) Å] and $(C_2H_5)_4N^+$ [4.381(1) Å] salts of the $Tl_2S_2(S_3)_2^{2-}$ anion,[29] which contains a planar Tl_2S_2 ring. The corresponding distance observed in the previously characterized (2,2,2-crypt-K^+)$_2Tl_2Te_2^{2-}$·en salt [3.600(3) Å][19] is significantly shorter than in the present structure and in $Tl_2Se_2^{2-}$ and is discussed below (see Computational Results). The Ch···Ch contacts observed in both anions [Se, 4.140(3) Å; Te, 4.552(2) Å] and in the previously characterized $Tl_2Te_2^{2-}$ anion [4.414(3) Å] are near the sums of the Se and Te van der Waals radii [Se, 4.0 Å; Te, 4.4 Å].[30]

The average Tl−Ch−Tl and Ch−Tl−Ch bond angles in the $Tl_2Se_2^{2-}$ anion [83.34(1) and 96.21(7)°, respectively] are closer to the 90° bond angles anticipated for a planar structure whereas those observed for $Tl_2Te_2^{2-}$ in (2,2,2-crypt-K^+)$_2Tl_2Te_2^{2-}$ [79.1(2) and 97.7(2)°] and in (2,2,2-crypt-K^+)$_2Tl_2Te_2^{2-}$·en [75.1(3) and 96.6(2)°] deviate from 90° to a greater extent. The angle trends observed in the $Tl_2Ch_2^{2-}$ anions, i.e., Se−Tl−Se < Te−Tl−Te and Tl−Se−Tl > Tl−Te−Tl, are in accord with the VSEPR rules[23] which predict that the Ch−Tl−Ch bond angles should decrease and the Tl−Ch−Tl bond angles should increase upon substitution with the more electronegative Se atom. Similar trends have been reported for the $M_2Ch_3^{2-}$ (M = Sn, Pb; Ch = S, Se, and/or Te) anion series.[31,32]

Structural Characterization of the $Tl_2Ch_2^{2-}$ (Ch = Se and/or Te) Anions by Solution NMR Spectroscopy. The $Tl_2Se_2^{2-}$ and Tl_2SeTe^{2-} anions have been previously characterized by ^{203}Tl and ^{205}Tl NMR spectroscopy at 24 °C in en solutions of the KTlSe and $KTlSe_{0.5}Te_{0.5}$ alloys containing 2,2,2-crypt and the $Tl_2Te_2^{2-}$ anion at −40 °C in a saturated liquid-NH_3 extract of KTlTe containing 2,2,2-crypt.[17] The spectra were exchange broadened ($\Delta\nu_{1/2} \sim 1000-3000$ Hz), and the $^2J(^{205}Tl-^{203}Tl)$ and $^1J(^{203,205}Tl-Ch)$ (Ch = ^{77}Se, ^{125}Te) couplings were poorly resolved. Moreover, no ^{77}Se NMR spectra were reported, and the ^{205}Tl NMR resonance of $Tl_2Te_2^{2-}$ could not be observed at temperatures above −40 °C. In the present work, the natural abundance and the ^{77}Se-enriched $Tl_2Se_2^{2-}$ anion (the ^{77}Se-enriched anion will hereafter be referred to as $Tl_2{}^{77}Se_2^{2-}$) and the $Tl_2Te_2^{2-}$ anion were characterized by variable-temperature ^{205}Tl, ^{203}Tl, and ^{77}Se NMR spectroscopy. The ^{203}Tl and ^{205}Tl NMR spectra of the $Tl_2Te_2^{2-}$ anion in a saturated liquid-NH_3 solution of KTlTe containing 2,2,2-crypt were also repeated at −70 °C, giving rise to $^2J(^{205}Tl-^{203}Tl)$ and $^1J(^{205}Tl-^{125}Te)$ values that are at variance with the previous values (see Table 4). Interestingly, no ^{125}Te resonances corresponding to the $Tl_2Te_2^{2-}$ anion could be observed in the present and previous studies.

The ^{203}Tl and ^{205}Tl NMR resonances corresponding to the known $TlCh_3^{3-}$ (Ch = Se or Te) anions[20] were also observed in the en and liquid-NH_3 alloy extracts at all temperatures with well-resolved Tl−Ch couplings. The chemical shifts and spin−spin coupling constants for the $TlCh_3^{3-}$ and $Tl_2Ch_2^{2-}$ anions are listed in Table 4.

(a) Chemical Exchange Behavior. The ^{205}Tl NMR spectrum of a solution of $Tl_2Se_2^{2-}$ obtained from an en extract of $KTlSe_{0.5}Te_{0.5}$ was recorded at 0 °C and gave rise to well resolved $^{205}Tl-^{203}Tl$ and $^{205}Tl-^{77}Se$ couplings. The ^{205}Tl NMR resonance of the Tl_2SeTe^{2-} anion was also observed but was exchange broadened ($\Delta\nu_{1/2} \sim 3000$ Hz) and precluded observation of all couplings. The ^{205}Tl and ^{203}Tl NMR spectra of Tl_2SeTe^{2-} sharpened upon cooling to −70 °C in liquid NH_3 ($\Delta\nu_{1/2} \sim 300$ Hz) and enabled a complete assignment of all nuclear spin−spin coupling constants. Interestingly, the −40 and −60 °C ^{205}Tl, ^{203}Tl, and ^{77}Se NMR spectra of $Tl_2Se_2^{2-}$ obtained from a liquid NH_3 extract of the KTlSe alloy were exchange broadened to such an extent ($\Delta\nu_{1/2} \sim 2500-3000$ Hz) that accurate measurements of $^{205}Tl-^{77}Se$ and $^{203}Tl-^{77}Se$ couplings were not possible, and only the $^{205}Tl-^{203}Tl$ coupling was resolved. The fully resolved ^{205}Tl, ^{203}Tl, and ^{77}Se NMR resonances of $Tl_2Se_2^{2-}$ as well as those of $Tl_2{}^{77}Se_2^{2-}$ were only observed in liquid NH_3 at −70 °C.

The ^{205}Tl NMR spectrum of the $Tl_2Te_2^{2-}$ anion was obtained at 0 °C in en and at −70 °C in liquid NH_3. Although the ^{205}Tl

(26) Toure, A. A.; Kra, G.; Eholie, R.; Olivier-Fourcade, J.; Jumas, J.-C. *J. Solid State Chem.* **1990**, *87*, 229.
(27) Schewe, I.; Böttcher, P.; von Schnering, H. G. *Z. Kristallogr.* **1989**, *118*, 287.
(28) Pearson, W. B. In *Handbook of Lattice Spacings and Structures of Metals*; Pergamon Press: Oxford, U.K., 1967; Bd. 2, S. 90.
(29) Dhingra, S. S.; Kanatzidis, M. G. *Inorg. Chem.* 1993, *32*, 2298.
(30) Pauling, L. *The Nature of the Chemical Bond*, 3rd ed.; Cornell University Press: Ithaca, NY, 1960; pp 224, 257, 260, 514.
(31) Björgvinsson, M.; Sawyer, J. F.; Schrobilgen, G. J. *Inorg. Chem.* **1987**, *26*, 741.
(32) Björgvinsson, M.; Mercier, H. P. A.; Mitchell, K. M.; Schrobilgen, G. J.; Strohe, G. *Inorg. Chem.* **1993**, *32*, 6046.

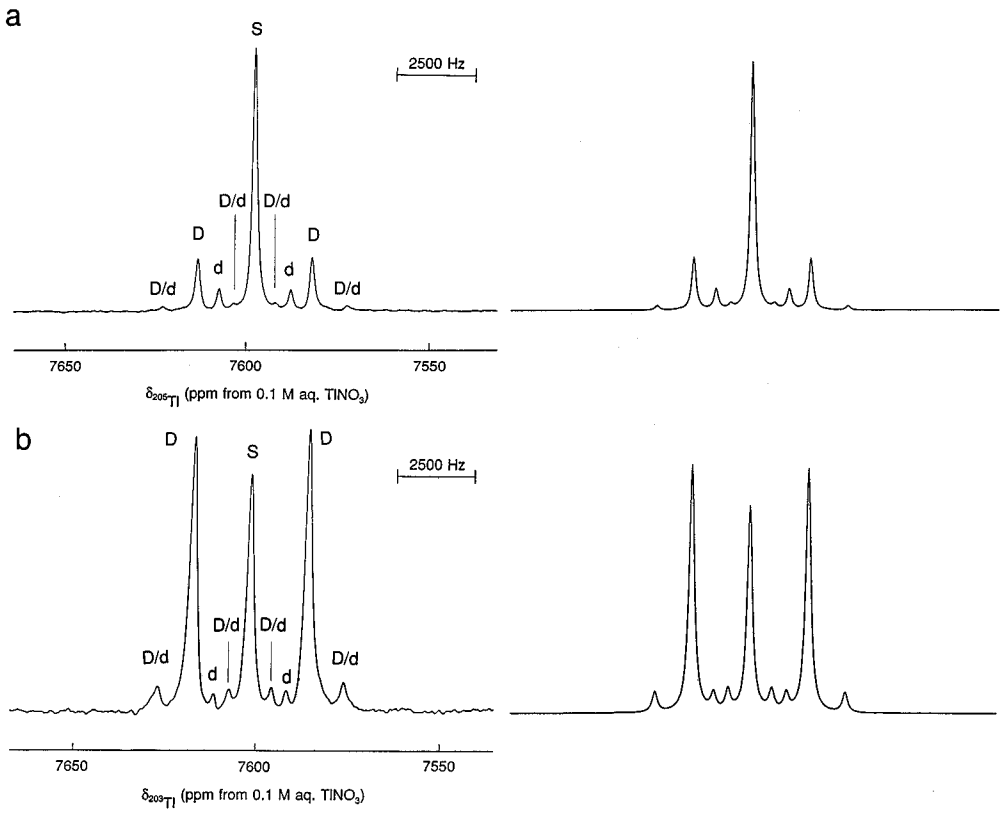

Figure 2. NMR spectra of the natural abundance $Tl_2Se_2^{2-}$ anion: (a) ^{205}Tl (115.444 MHz) and (b) ^{203}Tl (114.319 MHz) recorded in liquid NH_3 at −70 °C and simulated spectra (right-hand traces). The symbols used to label the peaks are defined in Table 5 and in the text.

resonances obtained at both temperatures were broad ($\Delta\nu_{1/2} \sim$ 1000 Hz), the $^{205}Tl-^{203}Tl$ and $^{205}Tl-^{125}Te$ couplings could be resolved.

From these findings, the lability in the series of $Tl_2Ch_2^{2-}$ anions increases in the order $Tl_2Se_2^{2-} < Tl_2SeTe^{2-} < Tl_2Te_2^{2-}$.

(b) Chemical Shifts. The ^{203}Tl and ^{205}Tl chemical shifts of the $Tl_2Ch_2^{2-}$ (Ch = Se and/or Te) anions (Table 4) appeared in the Tl^{I} region and contrast with those observed for the $TlCh_3^{3-}$ anions which appeared in the Tl(III) region. Similar ^{205}Tl chemical shifts have also been reported for the trigonal bipyramidal $TlSnTe_3^{3-}$ (4196 ppm) and $TlPbTe_3^{3-}$ (3438 ppm) anions in which the thallium atoms are formally in the +1 oxidation state.[33] On the basis of the higher electronegativity of Se when compared to that of Te,[34] the shielding of the thallium NMR resonances in the $Tl_2Ch_2^{2-}$ anion series is anticipated to increase in the order $Tl_2Te_2^{2-} > Tl_2SeTe^{2-} > Tl_2Se_2^{2-}$. This trend has been noted for the anion series $TlCh_3^{3-}$,[20] $SnCh_3^{2-}$,[20] $SnCh_4^{4-}$,[20] $Pb_2Ch_3^{2-}$,[31,32] $HgCh_2^{2-}$,[20] and $CdCh_3^{2-}$ [20] upon substitution with the more electronegative Se atom. Interestingly, the shielding trend observed for the $Tl_2Ch_2^{2-}$ anion series (Table 4) is the reverse of the anticipated order. A similar anomaly has also been noted for the $Sn_4Se_{10}^{4-}$ anion[35] in which the order, $\delta(^{77}Se_{terminal}) < \delta(^{77}Se_{bridging})$, anticipated on the basis of charge topology arguments[36] was reversed, but the anticipated order is exhibited for the related $Sn_2Se_6^{4-}$ and $Sn_2Te_6^{4-}$ anions.[21] It is also interesting to note that the Tl^{I} NMR resonances of the $Tl_2Ch_2^{2-}$ anions appear within a smaller chemical shift range (600 ppm) as do the $^{113}Cd^{II}$ chemical shifts of $CdCh_2^{2-}$ (400 ppm),[20] but larger chemical shift ranges are observed for $^{205}Tl^{III}$ in $TlCh_3^{3-}$ (2400 ppm),[20] $^{119}Sn^{IV}$ in $SnCh_3^{2-}$ (900 ppm) and $SnCh_4^{4-}$ (1350 ppm),[20] $^{207}Pb^{II}$ in $Pb_2Ch_3^{2-}$ (1600 ppm),[31,32] and $^{199}Hg^{II}$ in $HgCh_2^{2-}$ (1400 ppm).[20]

(c) Analysis of Spin−Spin Coupling Patterns. The experimental and simulated ^{205}Tl and ^{203}Tl NMR spectra of the $Tl_2Ch_2^{2-}$ anions (Ch = Se and/or Te) are depicted in Figures 2−5. Spectral simulations confirmed that the assigned satellite doublet spacings corresponded to $^1J(^{205}Tl-^{77}Se)$, $^1J(^{205}Tl-^{125}Te)$, and $^2J(^{205}Tl-^{203}Tl)$ at their natural abundance and 94.4% ^{77}Se-enriched levels and were consistent with a solution structure for the $Tl_2Ch_2^{2-}$ anions in which the thallium atoms and the chalcogen atoms are chemically equivalent.

The ^{205}Tl and ^{203}Tl NMR spectra of the $Tl_2Ch_2^{2-}$ and $Tl_2{}^{77}Se_2^{2-}$ anions were simulated by using the natural abundances of the spin-$^1/_2$ nuclides ^{205}Tl (70.5%), ^{203}Tl (29.5%), ^{77}Se (7.58%; isotopically enriched, 94.4%), and ^{125}Te (6.99%),[37] the values of the observed coupling constants, and the total line intensities and multiplicities of the most abundant isotopomers contributing significant first-order subspectra to the experimental ^{205}Tl and ^{203}Tl NMR spectra (Table 5). The resulting simulations (Figures 2−5) are in excellent agreement with the experimental spectra and account for all the observed satellite peaks.

The −70 °C ^{205}Tl NMR spectrum (Figure 2a) of the natural-abundance $Tl_2Se_2^{2-}$ anion consists of a SINGLET (S) flanked by DOUBLET (D) satellites arising from $^2J(^{205}Tl-^{203}Tl) = 3602$ Hz and doublet (d) satellites arising from $^1J(^{205}Tl-^{77}Se) = 2261$ Hz. In addition, four weaker satellites also symmetrically disposed about the central peak were observed and are assigned

(33) Borrmann, H.; Campbell, J.; Dixon, D. A.; Mercier, H. P. A.; Pirani, A. M.; Schrobilgen, G. J. *Inorg. Chem.*, submitted for publication.
(34) Allen, L. C. *J. Am. Chem. Soc.* **1989**, *111*, 9003 and references therein.
(35) Campbell, J.; DiCiommo, D. P.; Mercier, H. P. A.; Pirani, A. M.; Schrobilgen, G. J. *Inorg. Chem.* **1995**, *34*, 6265.
(36) Gimarc, B. M.; Ott, J. J. *J. Am. Chem. Soc.* **1986**, *108*, 4298.
(37) Mason, J. In *Multinuclear NMR*; Mason, J., Ed.; Plenum Press: New York, 1987; Appendix, pp 626−627.

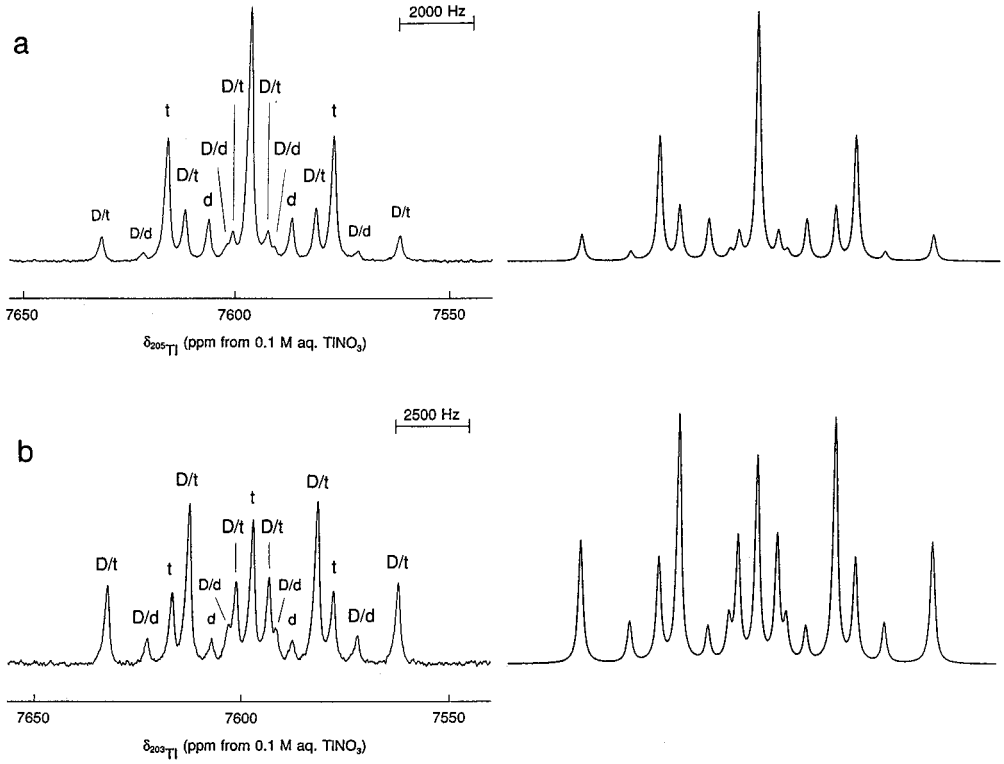

Figure 3. NMR spectra of the ^{77}Se-enriched $Tl_2Se_2^{2-}$ anion recorded in liquid NH_3 at −70 °C and simulated spectra (right-hand traces): (a) ^{205}Tl (115.444 MHz) and (b) ^{203}Tl (114.319 MHz). The symbols used to label the peaks are defined in Table 5 and in the text.

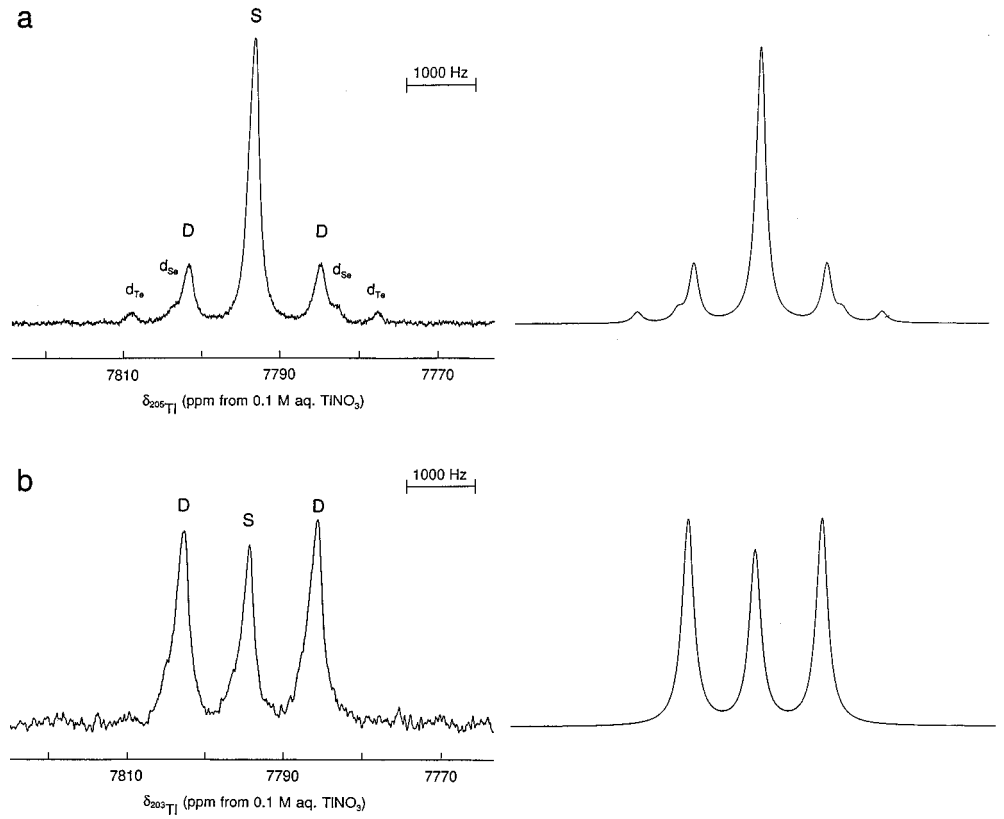

Figure 4. NMR spectra of the Tl_2SeTe^{2-} anion recorded in liquid NH_3 at −70 °C: (a) ^{205}Tl (115.444 MHz) and (b) ^{203}Tl (114.319 MHz). The symbols used to label the peaks are defined in Table 5 and in the text.

to a DOUBLET-of-doublets (D/d) subspectrum arising from the $^{205}Tl^{203}Tl^{77}Se^{0}Se^{2-}$ isotopomer (Table 5). The DOUBLET arises from $^{2}J(^{205}Tl-^{203}Tl)$ coupling and is further split into a doublet by $^{1}J(^{205}Tl-^{77}Se)$. The corresponding coupling, $^{1}J(^{203}Tl-^{77}Se) = 2254$ Hz, was determined by recording the ^{203}Tl NMR spectrum (Figure 2b) in which the ^{205}Tl satellites are more intense than the central peak owing to the greater natural abundance of the ^{205}Tl nuclide (70.5%) when compared with that of ^{203}Tl (29.5%).[37] The ratio $^{1}J(^{205}Tl-^{77}Se)/^{1}J(^{203}Tl-^{77}Se) = 1.030$ is in excellent agreement with the ratio

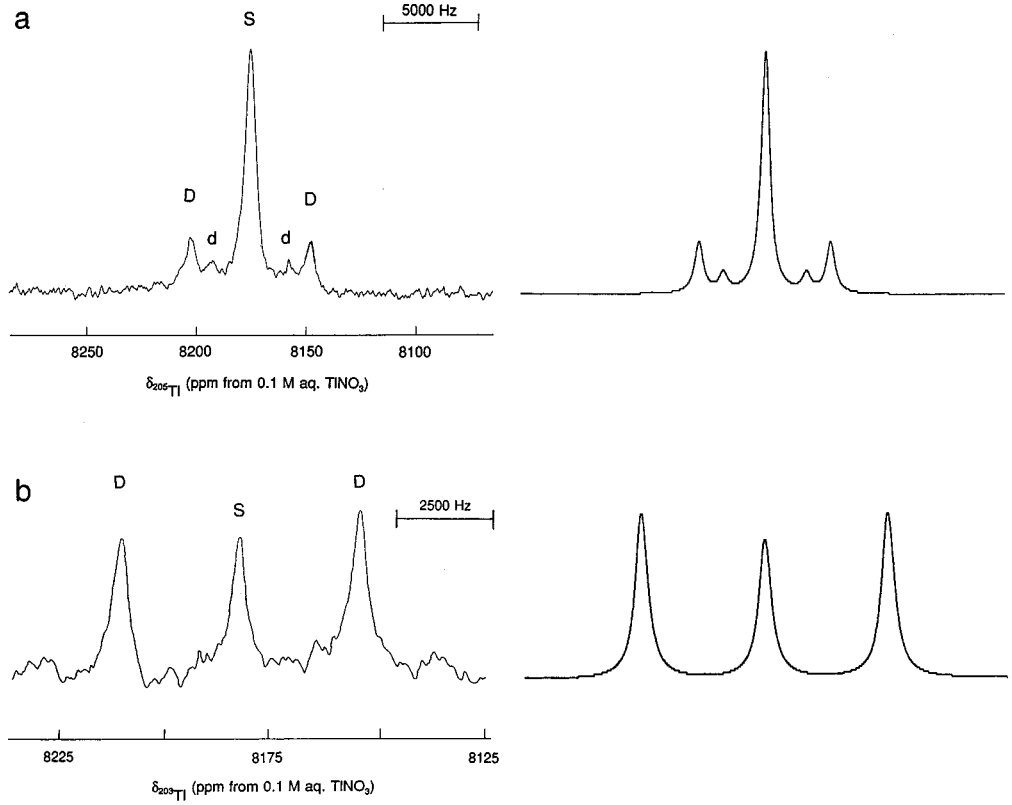

Figure 5. NMR spectra of the $Tl_2Te_2^{2-}$ anion recorded in en at 0 °C: (a) ^{205}Tl (115.444 MHz) and (b) ^{203}Tl (114.319 MHz). The symbols used to label the peaks are defined in Table 5 and in the text.

of the gyromagnetic ratios of the ^{205}Tl and ^{203}Tl nuclides, $\gamma(^{205}Tl)/\gamma(^{203}Tl) = 1.010$. The ^{205}Tl NMR spectrum of $Tl_2{}^{77}Se_2^{2-}$ consists of the superposition of four isotopomeric subspectra (Figure 3a). The most intense ^{205}Tl subspectrum is that of the $^{205}Tl_2{}^{77}Se_2^{2-}$ isotopomer and is a triplet (t) arising from $^1J(^{205}Tl-^{77}Se)$. The spectrum of the second most abundant isotopomer, $^{205}Tl^{203}Tl^{77}Se_2^{2-}$, is a DOUBLET attributed to $^2J(^{205}Tl-^{203}Tl)$, whose transitions are further split into a triplet by $^1J(^{205}Tl-^{77}Se)$. The next most abundant isotopomer, $^{205}Tl^{203}Tl^{77}Se^0Se^{2-}$, gives rise to a DOUBLET subspectrum corresponding to $^2J(^{205}Tl-^{203}Tl)$, which, in turn, is split into a doublet arising from $^1J(^{205}Tl-^{77}Se)$. The least detectable isotopomer is $^{205}Tl_2{}^0Se^{77}Se$ and gives rise to a doublet arising from $^1J(^{205}Tl-^{77}Se)$. The ^{203}Tl NMR spectrum (Figure 3b) consists of a similar pattern; however, the relative isotopomer line intensities (Table 5) differ significantly from those of the ^{205}Tl NMR spectrum because of the different natural abundances of the two spin-active thallium nuclides. The ^{77}Se NMR resonance of natural-abundance and ^{77}Se-enriched $Tl_2Se_2^{2-}$ anion is a triplet attributed to unresolved $^1J(^{77}Se-^{203}Tl)$ and $^1J(^{77}Se-^{205}Tl)$ couplings.

The ^{205}Tl NMR spectrum of the Tl_2SeTe^{2-} anion (Figure 4a) consists of a broad singlet flanked by three sets of symmetric satellites attributed to $^1J(^{205}Tl-^{77}Se)$, $^1J(^{205}Tl-^{125}Te)$, and $^2J(^{205}Tl-^{203}Tl)$. The ^{205}Tl NMR spectrum of $Tl_2Te_2^{2-}$ consists of a broad singlet and symmetric $^1J(^{205}Tl-^{125}Te)$ and $^2J(^{205}Tl-^{203}Tl)$ satellites (Figure 5a). The counterparts of the four weaker satellites [i.e., DOUBLET-of-doublets (D/d) in Figure 2a] observed in the ^{205}Tl NMR spectrum of natural abundance $Tl_2Se_2^{2-}$ were not observed in the ^{205}Tl NMR spectra of Tl_2SeTe^{2-} and $Tl_2Te_2^{2-}$ owing to exchange broadening of the multiplet lines ($\Delta\nu_{1/2} \sim 500$ Hz). The ^{203}Tl NMR spectra of the Tl_2SeTe^{2-} (Figure 4b) and $Tl_2Te_2^{2-}$ (Figure 5b) anions consisted of singlets symmetrically flanked by ^{205}Tl satellites.

Table 5. Isotopomers and Subspectra Used To Simulate the ^{205}Tl and ^{203}Tl NMR Spectra of the $Tl_2Ch_2^{2-}$ (Ch = Se and/or Te) Anions

	relative intensity[b]				
	^{205}Tl		^{203}Tl		multiplicity of subspectrum[c]
isotopomer[a]	Se	Te	Se	Te	
Natural Abundance $Tl_2Ch_2^{2-}$					
$^{205(203)}Tl_2{}^0Ch_2^{2-}$	0.8487	0.8598	0.1486	0.1505	S
$^{205}Tl^{203}Tl^0Ch_2^{2-}$	0.3551	0.3598	0.3551	0.3598	D
$^{205(203)}Tl_2{}^{77}Ch^0Ch^{2-}$	0.1396	0.1292[d]	0.02444[d]	0.0226[d]	d
$^{205}Tl^{203}Tl^{77}Ch^0Ch^{2-}$	0.05842[d]		0.05842		D/d
Isotopically Enriched $Tl_2Se_2^{2-}$					
$^{205(203)}Tl_2{}^{77}Se_2^{2-}$	0.8858		0.1551		t
$^{205}Tl^{203}Tl^{77}Se_2^{2-}$	0.3707		0.3707		D/t
$^{205(203)}Tl_2{}^{77}Se^0Se^{2-}$	0.1051		0.01840[d]		[d]
$^{205}Tl^{203}Tl^{77}Se^0Se^{2-}$	0.04398[d]		0.04398		D/d
Natural Abundance Tl_2SeTe^{2-}					
$^{205(203)}Tl_2{}^0Se^0Te^{2-}$	0.8542		0.1496		S
$^{205}Tl^{203}Tl^0Se^0Te^{2-}$	0.3574		0.3576		D
$^{205(203)}Tl_2{}^{77}Se^0Te^{2-}$	0.07026		0.01227		d_{Se}
$^{205(203)}Tl_2{}^0Se^{125}Te^{2-}$	0.06430[d]		0.01124[d]		d_{Te}

[a] The symbols ^0Ch, ^0Se, and ^0Te denote spinless chalcogen atoms. [b] Natural abundances of the spin−$^1/_2$ nuclides used to calculate isotopomer intensities were taken from ref 34: ^{77}Se (natural abundance, 7.58%; enriched, 94.4%); ^{125}Te, 6.99%; ^{203}Tl, 29.5%; ^{205}Tl, 70.5%. The natural abundance of ^{123}Te (0.87%) is too low to contribute detectable isotopomer subspectra and is combined with the spinless tellurium. [c] S denotes a SINGLET, D denotes a DOUBLET arising from $J(^{205}Tl-^{203}Tl)$, and d and t denote doublets and triplets arising from $^1J(^{205(203)}Tl-{}^*Ch)$ and $^1J(^{205(203)}Tl-{}^*Ch_2)$, respectively, where *Ch represents ^{77}Se or ^{125}Te. The symbols D/d and D/t denote DOUBLET-of-doublets and DOUBLET-of-triplets, respectively, that result from a DOUBLET which, in turn, is split either into a doublet or a triplet. [d] Isotopomer having multiplet line intensities below this value are too weak to be observed and are not included in the summation of the simulated subspectra.

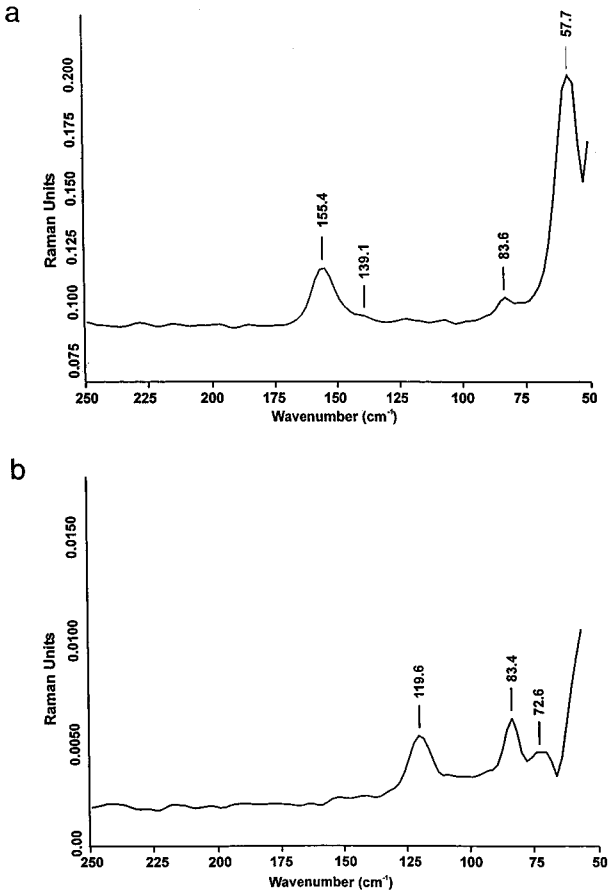

Figure 6. Raman spectra of (a) $Tl_2Se_2^{2-}$ and (b) $Tl_2Te_2^{2-}$ in (2,2,2-crypt-K^+)$_2Tl_2Ch_2^{2-}$ (Ch = Se or Te) recorded in a glass capillary on powdered samples at room temperature by using a 1064-nm excitation of a Nd YAG laser.

The corresponding $^1J(^{203}Tl-^{77}Se)$ and $^1J(^{203}Tl-^{125}Te)$ couplings could not be observed.

The Tl−Tl couplings observed in the $Tl_2Ch_2^{2-}$ (Ch = Se and/or Te) anions show a high degree of variability with environmental changes such as temperature, solvent, and nature of the countercation (Table 4), whereas the Tl−Ch couplings in all three anions are relatively insensitive to the environmental changes. For example, the Tl−Tl couplings observed for $Tl_2Se_2^{2-}$ in liquid-NH_3 solvent decreased from 3995 to 3602 Hz (*ca.* 10%) when the temperature was decreased from -40 to −70 °C, but Tl−Se couplings for the anion varied by only 50 Hz (*ca.* 2%). The variability in the Tl−Tl coupling constant for the $Tl_2Te_2^{2-}$ anion was significantly more pronounced (*ca.* 17%); however, the Tl−Te couplings varied only by *ca.* 5% under similar experimental conditions. This suggests that the $Tl_2Ch_2^{2-}$ anions are easily deformed about the fold angles (see Computational Results).

Raman Spectra of the $Tl_2Ch_2^{2-}$ (Ch = Se, Te) Anions. The solid-state Raman spectra of the anions in (2,2,2-crypt-K^+)$_2Tl_2Se_2^{2-}$ and (2,2,2-crypt-K^+)$_2Tl_2Te_2^{2-}$ are shown in Figure 6. The observed frequencies were assigned with the aid of LDFT and NLDFT calculations, and their assignments are summarized in Table 6 along with their theoretical values and the theoretical values of the Tl_2SeTe^{2-} anion (see Computational Results). Assignments for the 2,2,2-crypt-K^+ cation were made by comparison with values reported for the solid-state Raman spectra of (2,2,2-crypt-K^+)I- and require no further discussion.[38]

The vibrational modes of the $Tl_2Ch_2^{2-}$ anions were assigned under C_{2v} point symmetry of the butterfly structure in which

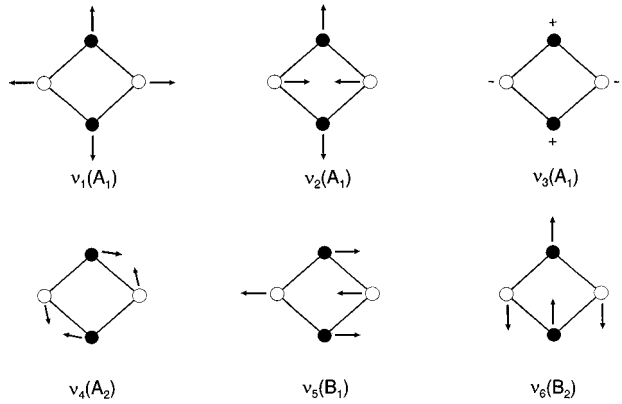

Figure 7. Vibrational modes of the $Tl_2Ch_2^{2-}$ (Ch = Se or Te) anions.

the Tl atoms lie in the $\sigma(xz)$-plane and the Ch atoms lie in the $\sigma(yz)$-plane and belong to the irreducible representation $3A_1 + A_2 + B_1 + B_2$. A total of 6 vibrational bands is expected, of which all modes are Raman active and three (A_1, B_1, B_2) are infrared active. Descriptions of the vibrational modes of the $Tl_2Ch_2^{2-}$ anions were derived from LDFT and NLDFT calculations and are depicted in Figure 7. The highest frequency mode, $\nu_1(A_1)$, corresponds to the symmetric breathing motion of the ring. The asymmetric combination of the Tl···Tl and Ch···Ch motions, $\nu_2(A_1)$, is at much lower frequency. The lowest totally symmetric mode, $\nu_3(A_1)$, is the inversion mode. The $\nu_4(A_2)$ mode corresponds to the simultaneous shortening (lengthening) of two nonadjacent Tl−Ch bonds and the lengthening (shortening) of the remaining two Tl−Ch bonds. The $\nu_5(B_1)$ mode corresponds to the displacement of both Tl atoms in the positive direction along the *x*-axis and the displacement of both Ch atoms in the negative *x*-direction parallel to the *x*-axis. For the $\nu_6(B_2)$ mode, the two Ch atoms are displaced in the positive direction along the *y*-axis and the Tl atoms are displaced in the negative *y*-direction parallel to the *y*-axis.

It was not possible to observe all the Raman bands for $Tl_2Se_2^{2-}$ and $Tl_2Te_2^{2-}$. In general, the $Tl_2Te_2^{2-}$ anion modes are shifted to lower frequency relative to those of $Tl_2Se_2^{2-}$ by virtue of the reduced mass effect. For both anions, the assignments of the $\nu_1(A_1)$ vibrations are unambiguous and the $\nu_2(A_1)$, $\nu_3(A_1)$ and $\nu_5(B_1)$, $\nu_6(B_2)$ bands are expected to be near degenerate on the basis of theoretical calculations. In the case of $Tl_2Se_2^{2-}$, the $\nu_5(B_1)$ and $\nu_6(B_2)$ bands overlap, are weak in comparison with $\nu_1(A_1)$, and are unambiguously assigned to the band at 139 cm^{-1} on the basis of calculated values. The $\nu_5(B_1)$ and $\nu_6(B_2)$ modes of $Tl_2Te_2^{2-}$ are also predicted to be similar in frequency to the more intense $\nu_1(A_1)$ band at 120 cm^{-1} and likely overlap with this band. A band at 73 cm^{-1} in the Raman spectrum of $Tl_2Te_2^{2-}$ is tentatively assigned to the $\nu_2(A_2)$ and $\nu_3(A_1)$ modes of the anion but could be alternatively assigned to a lattice mode because it is significantly higher in frequency than its counterparts in the $Tl_2Se_2^{2-}$ anion and its calculated values. The experimental $\nu_4(A_2)$ modes of both anions are similar and are in reasonable agreement with their calculated values.

Computational Results. In order to better understand the structures, properties, and spectra of the $Tl_2Ch_2^{2-}$ (Ch = Se and/or Te) anions, DFT calculations were performed. The

(38) The Raman spectrum of microcrystalline (2,2,2-crypt-K^+)I^- displayed several very weak, broad bands in the 50−350 cm^{-1} region.[21] The most intense 2,2,2-crypt-K^+ band at 135 cm^{-1}, which probably overlaps with the $Tl_2Ch_2^{2-}$ bands (Table 6), was too weak to be observed in the Raman spectrum of (enH^+)$_2$(2,2,2-crypt-K^+)$_2Sn_2Se_6^{4-}$.[21]

Table 6. Experimental and Calculated Vibrational Frequencies and Assignments for the $Tl_2Ch_2^{2-}$ (Ch = Se, Te) Anions

frequencies (cm^{-1})						
	LDFT[b]		NLDFT[b]			
exptl[a]	PP/PP	PP/DZVP	PP/PP	PP/DZVP	LDFT[b] ECP	assigts in C_{2v} pt sym
			$Tl_2Se_2^{2-}$			
155 (24)	159 (4)	163 (3)	151 (4)	156 (3)	153 (7)	$\nu_1(A_1)$
	72 (0)	56 (0)	72 (0)	56 (0)	62 (0)	$\nu_2(A_1)$
58 (100)	62 (0)	38 (5)	61 (1)	43 (5)	35 (4)	$\nu_3(A_1)$
84 (8)	94 (0)	107 (0)	84 (0)	98 (0)	91 (0)	$\nu_4(A_2)$
139 sh	146 (29)	150 (26)	139 (31)	144 (25)	143 (48)	$\nu_5(B_1)$
	145 (24)	161 (55)	140 (24)	153 (56)	143 (27)	$\nu_6(B_2)$
			$Tl_2Te_2^{2-}$			
120 (100)	123 (3)	130 (4)	118 (3)	123 (3)	119 (2)	$\nu_1(A_1)$
73 (20)	58 (0)	47 (0.5)	57 (0)	45 (0)	49 (0)	$\nu_2(A_1)$
	51 (0)	34 (2)	49 (0)	33 (2)	26 (2)	$\nu_3(A_1)$
84 (85)	78 (0)	90 (0)	70 (0)	81 (0)	76 (0)	$\nu_4(A_2)$
	116 (20)	130 (40)	110 (22)	122 (43)	116 (35)	$\nu_5(B_1)$
120 (100)	114 (10)	118 (13)	110 (10)	113 (13)	109 (10)	$\nu_6(B_2)$

Tl_2SeTe^{2-}

frequencies (cm^{-1})				frequencies (cm^{-1})			
LDFT[b] PP/PP	NLDFT[b] PP/PP	LDFT[b] ECP	assgnts in C_s pt sym	LDFT[b] PP/PP	NLDFT[b] PP/PP	LDFT[b] ECP	assgnts in C_s pt sym
156 (14)	151 (4)	153 (7)	$\nu_1(A')$	94 (0)	84 (0)	91 (0)	$\nu_4(A')$
72 (0)	72 (0)	62 (0)	$\nu_2(A')$	146 (29)	139 (31)	143 (48)	$\nu_5(B'')$
62 (0)	61 (1)	35 (4)	$\nu_3(A')$	145 (24)	140 (24)	143 (27)	$\nu_6(B'')$

[a] The Raman spectra were recorded in glass capillaries on powdered samples at room temperature by using a 1064-nm excitation of a Nd YAG laser. Relative intensities are given in parentheses. [b] The calculated relative line intensities, in km mol^{-1}, are given in parentheses.

Table 7. Calculated Vibrational Frequencies, Geometric Parameters, Charges, Mayer Valencies, and Bond Orders for the $In_2Ch_2^{2-}$ (Ch = Se, Te) Anions

	$In_2Se_2^{2-}$		$In_2Te_2^{2-}$		
	VWN/DZVP	VWN/PP/PP	VWN/DZVP	VWN/PP/PP	assignts (C_{2v})
			Frequencies (cm^{-1})		
	185 (3)	167 (2)	148 (3)	135 (2)	$\nu_1(A_1)$
	88 (0)	84 (0)	61 (0)	64 (0)	$\nu_2(A_1)$
	38 (0)	38 (0)	34 (0)	43 (0)	$\nu_3(A_1)$
	136 (0)	106 (0)	110 (0)	88 (0)	$\nu_4(A_1)$
	181 (49)	159 (29)	143 (23)	127 (13)	$\nu_5(B_1)$
	178 (28)	157 (19)	144 (26)	127 (13)	$\nu_6(B_2)$
			Geometric Parameters		
In···In (Å)	3.597	3.703	3.782	3.796	
In−X (Å)	2.687	2.772	2.916	2.953	
X···X (Å)	3.904	4.021	4.268	4.320	
In−X−In (deg)	84.0	83.8	80.9	80.0	
X−In−X (deg)	93.2	93.0	94.1	94.0	
fold angle (deg)[a]	24.4	25.9	32.2	34.5	
			Charges		
In	−0.42	−0.43	−0.41	−0.45	
X	−0.58	−0.57	−0.59	−0.55	
			Valencies		
In	2.30	2.29	2.18	2.30	
X	1.97	2.20	1.96	2.26	
			Bond Orders		
In···In	0.38	0.20	0.25	0.17	
Tl−X	0.96	1.05	0.97	1.07	
X···X	0.04	0.11	0.02	0.12	

[a] The fold angle in the anion structures is the dihedral angle between the two In_2Ch planes.

calculations were used to assign the vibrational spectra of $Tl_2Se_2^{2-}$ and $Tl_2Te_2^{2-}$, to gain insight into the extent to which the anion environment influences the fold angle at the Tl−Tl axis, and to better understand the nature of bonding and the relative magnitudes of the Tl−Ch and Tl−Tl NMR spin−spin couplings.

(a) Geometries of and Bonding in the $In_2Ch_2^{2-}$ and $Tl_2Ch_2^{2-}$ (Ch = Se and/or Te) Anions. In order to understand the behavior of the various basis set treatments used in this study, calculations for the presently unknown $In_2Se_2^{2-}$ and $In_2Te_2^{2-}$ anions, for which all-electron basis sets are available, are also included in this study (Table 7). The calculations for $In_2Te_2^{2-}$ show reasonable agreement between the geometric parameters calculated by using all-electron and pseudopotential (PP) treatments with the PP calculation showing a slightly expanded structure. Agreement is not as good for the $In_2Se_2^{2-}$ anion with the interatomic distances being approximately 0.10 Å longer than the all-electron values. The structures calculated by using an all-electron basis set for Se or Te and a pseudopotential on Tl (P, all) are not in good agreement with other calculations or with experiment, giving predicted Tl−Ch and Ch···Ch distances which are too long (Table 3). Consequently,

Table 8. Charges (e) in the $Tl_2Ch_2^{2-}$ (Ch = Se, Te) Anions

	LDFT		NLDFT		
atom	PP/PP	PP/DZVP	PP/PP	PP/DZVP	LDFT[a] ECP
			$Tl_2Se_2^{2-}$		
Tl	−0.29	−0.08	−0.26	−0.08	−0.11 (0.12)
Se	−0.71	−0.92	−0.74	−0.92	−0.89 (−1.12)
			$Tl_2Te_2^{2-}$		
Tl	−0.32	−0.11	−0.29	−0.11	0.00 (0.06)
Te	−0.68	−0.89	−0.71	−0.89	−1.00 (−1.06)

Tl_2SeTe^{2-}

atom	LDFT PP/PP	NLDFT PP/PP	LDFT[a] ECP/DZVP
Tl	−0.30	−0.27	−0.06 (0.08)
Se	−0.69	−0.72	−0.85 (−1.10)
Te	−0.71	−0.74	−1.02 (−1.05)

[a] Natural bond order populations are given in parentheses.

the PP/PP results have been used, unless otherwise indicated, in the ensuing discussion of $Tl_2Ch_2^{2-}$.

The geometry derived for $Tl_2Se_2^{2-}$ is in good agreement with the experimental one at the LDFT and NLDFT levels when pseudopotentials are used for both Tl and Se (PP/PP). The Tl−Se distance is 0.03−0.04 Å too short (Table 3), whereas the Tl···Tl and Se···Se distances are too short by larger amounts (∼0.15 Å). Similar calculations for Pb_9^{3-} and Pb_9^{4-} also underestimated the Pb···Pb distances.[22] As a consequence, the calculated Tl−Se−Tl bond angle is too small and the calculated Se−Tl−Se angle is too large by ∼3° when compared to the experimental values. The calculated fold angle of 34° clearly shows that the optimum geometry is nonplanar. However, this fold angle also indicates that the structure is clearly not tetrahedral. The LDFT/PP/PP and NDLFT/PP/PP values are in reasonable agreement with each other, with the NDLFT values being slightly larger than the LDFT values and showing slightly better agreement with the experimental values (Table 3). Calculations with an all-electron basis set for Se produced a structure with a Tl···Tl distance closer to the experimental distance, but the Tl−Se and Se···Se distances are too long.

The $Tl_2Se_2^{2-}$ anion charge is largely localized on the more electronegative Se atoms (−0.7 e) with the remainder on the Tl atoms (−0.3 e) (Table 8). The calculated Mayer valencies[39] give values of 2 for Tl and Se, consistent with two Se atoms bonded to each Tl atom (Table 9). The mixed basis set results give larger separations for both anions. The Mayer bond order[39] between the Tl and Se atoms is just under 1 (0.95). There are weak interactions between the two Tl atoms (bond order, 0.14−0.15) and between the two Se atoms (bond order, 0.13−0.14). In order to show that these interactions were not exaggerated because of the predicted short Tl···Tl distance, bond orders were calculated from the experimental geometry and resulted in values of 0.12 for Tl···Tl and 0.15 for Se···Se, confirming that the presence of these interactions is not due to the use of the shorter calculated Tl···Tl distance.

The calculated results for $Tl_2Te_2^{2-}$ follow the same trends as those of $Tl_2Se_2^{2-}$, and the differences between the calculated and experimental values for the present $Tl_2Te_2^{2-}$ structure are similar to those obtained for $Tl_2Se_2^{2-}$ (Table 3). The calculated Tl−Te distance at the VWN/PP/PP level is slightly shorter than the experimental value. The Tl−Te−Tl angle is predicted to be ∼2° smaller than the experimental value, and the Te−Tl−Te bond angle is predicted to be about ∼5° larger. The fold angle is predicted to be larger in $Tl_2Te_2^{2-}$ (37.0°) than in $Tl_2Se_2^{2-}$ (33.8°). Mayer valencies and bond orders[39] for the $Tl_2Te_2^{2-}$ structures are similar to those predicted for $Tl_2Se_2^{2-}$ (Table 9), and use of the experimental geometry does not change the conclusion about the presence of weak Tl···Tl (bond order, 0.13-0.15) and Te···Te (bond order, 0.14−0.16) interactions. With the exception of the fold angle, the present experimental structure of $Tl_2Te_2^{2-}$ is a better approximation of the gas-phase geometry than that previously determined in the crystal structure of $(2,2,2\text{-crypt-}K^+)_2Tl_2Te_2^{2-}\cdot en$[19] (see Vibrational Frequencies). Comparison of the Tl···Tl and Te···Te distances reported for $(2,2,2\text{-crypt-}K^+)_2Tl_2Te_2^{2-}\cdot en$ with the calculated values shows that the experimental values are shorter than the calculated values by ∼0.15 Å and contrasts with the present structural determinations of $Tl_2Se_2^{2-}$ and $Tl_2Te_2^{2-}$ which give experimental Tl···Tl and Ch···Ch distances that are longer than the calculated values by the same amount.

Calculations were also performed on the Tl_2SeTe^{2-} anion (Tables 3, 8, and 9) at the all PP and ECP levels. The geometric parameters are as expected from the $Tl_2Se_2^{2-}$ and $Tl_2Te_2^{2-}$ anions. The fold angle is somewhat larger than that for the $Tl_2Se_2^{2-}$ anion and is more like that of $Tl_2Te_2^{2-}$. The ECP structure is flatter and has longer bond lengths. The electronic structure parameters and vibrational frequencies are as expected on the basis of the above results.

The presence of weak interactions between the Tl atoms is validated by even larger In···In interactions calculated for $In_2Se_2^{2-}$ and $In_2Te_2^{2-}$ using all-electron DZVP basis sets (Table 7) and indicates that the use of pseudopotentials is not biasing the predicted magnitudes of the Tl···Tl interactions. The Ch···Ch interactions calculated for $In_2Ch_2^{2-}$ are, however, significantly weaker than those calculated for the $Tl_2Ch_2^{2-}$ anions.

The dependence of the calculated results on the form of the treatment of the core electrons was checked by using effective core potentials. The ECP results for the geometry of $Tl_2Se_2^{2-}$ do not differ significantly from the LDFT/PP/PP results, except that now the predicted Tl−Se and Se···Se distances are slightly longer than the experimental ones. However, the fold angle is not changed significantly. The calculated frequencies at the ECP level are similar to the PP results except that the inversion frequency is lower at the ECP level by almost a factor of 2 (see Vibrational Frequencies). The results for $Tl_2Te_2^{2-}$ at the ECP level are similar. As in the case of $Tl_2Se_2^{2-}$, the Tl−Te and Te···Te distances are longer at the ECP level when compared to the experimental values. The ECP calculation favors an even more planar structure and a larger Te−Tl−Te bond angle, which is consistent with the crystal structure of $Tl_2Te_2^{2-}$ reported in this work, than do the PP calculations.

The ECP results were also analyzed by using the natural bond orbital (NBO) method of Weinhold and co-workers.[40] The NBO atomic populations (Table 10) show more ionicity as compared to the Mulliken charges. This is more pronounced for $Tl_2Se_2^{2-}$ than for $Tl_2Te_2^{2-}$. The NBO populations indicate that the Tl atoms carry slightly positive charges. The ECP results show larger charge differences than do the PP results with the largest differences found for $Tl_2Se_2^{2-}$. The NBO analyses were used to further assess the bonding in the anions (Table 11). The analysis shows four two-center Tl−Se bonds with populations of 1.96 e. The remaining bond population is in the σ^* orbital.

(39) Mayer, I. *Chem. Phys. Lett.* **1983**, *97*, 270; *Theoret. Chim. Acta* **1985**, *67*, 315; *Int. J. Quantum Chem.* **1986**, *29*, 73.

(40) (a) Reed, A. E.; Curtiss, L. A.; Weinhold, F. *Chem. Rev.* **1988**, *88*, 899. (b) Foster, J. P.; Weinhold, F. J. *J. Am. Chem. Soc.* **1980**, *102*, 7211. (c) Reed, A. E.; Weinhold, F. *J. Chem. Phys.* **1983**, *78*, 4066. (d) Reed, A. E.; Weinstock, R. B.; Weinhold, F. *J. Chem. Phys.* **1985**, *83*, 735. (e) Reed, A. E.; Weinhold, F. *J. Chem. Phys.* **1985**, *83*, 1736.

Table 9. Mayer Valencies and Mayer Bond Orders in the $Tl_2Ch_2^{2-}$ (Ch = Se, Te) Anions[a]

	LDFT			NLDFT	
	PP/PP	PP/DZVP	PP/DZVP	PP/PP	PP/DZVP
			$Tl_2Se_2^{2-}$		
Valencies					
Tl	2.04 (2.00)	(1.75)	1.72	2.00	1.71
Se	2.03 (2.01)	(1.69)	1.67	1.99	1.66
Bond Orders					
Tl···Tl	0.15 (0.12)	(0.12)	0.14	0.14	0.13
Tl−Se	0.95 (0.93)	(0.82)	0.79	0.93	0.88
Se···Se	0.14 (0.15)	(0.055)	0.09	0.13	0.08
			$Tl_2Te_2^{2-}$		
Valencies					
Tl	2.12 (2.07) [2.11]	1.79 (1.83) [1.86]		2.07	1.76
Te	2.13 (2.09) [2.11]	1.72 (1.76) [1.77]		2.08	1.70
Bond Orders					
Tl···Tl	0.15 (0.16) [0.15]	0.14 (0.13) [0.13]		0.13	0.14
Tl−Te	0.99 (0.96) [0.98]	0.82 (0.85) [0.87]		0.97	0.82
Te···Te	0.16 (0.18) [0.16]	0.07 (0.06) [0.04]		0.14	0.07

Tl_2SeTe^{2-}

	LDFT PP/PP	NLDFT PP/PP		LDFT PP/PP	NLDFT PP/PP
Valencies			Bond Orders		
Tl	2.08	2.03	Tl···Tl	0.15	0.13
Se	2.06	2.02	Tl−Se	0.96	0.94
Te	2.09	2.04	Tl−Te	0.97	0.95
			Te···Te	0.15	0.14

[a] Values reported in parentheses refer to the structure reported in this work, whereas those in brackets refer to the structure reported in ref 19.

Table 10. Natural Atomic Orbital Populations in the $Tl_2Ch_2^{2-}$ (Ch = Se, Te) Anions at the Effective Core Potential Level

	Se	Te	Se/Te
Tl (s)	1.89	1.94	1.92
Tl (p_y)	0.47	0.33	0.34
Tl (p_x)	0.28	0.43	0.29
Tl (p_z)	0.26	0.24	0.45
Ch (s)	1.89	1.91	1.90/1.90
Ch (p_y)	1.68	1.64	1.73/1.62
Ch (p_x)	1.73	1.72	1.75/1.81
Ch (p_z)	1.78	1.78	1.71/1.71

The two-center Tl−Se bond has 84% of the two electrons on Se and 16% on Tl. The bonding is predominantly p in character with 95% p character on Tl and 89% p character on Se. For $Tl_2Te_2^{2-}$, the bonding pattern is the same with 82% of the bond localized on Te and 18% on Tl. The p character on Te is 90%, and that on Tl is 95%. The remaining valence electrons are found in lone pairs. There is essentially a doubly occupied lone pair of high s-orbital character on each thallium and chalcogen atom. This accounts for all except four of the valence electrons. These remaining electrons are predominantly in the Se lone pair which has 1.82 electrons and is predominantly an "out-of-plane" p orbital, although there is some population in the p orbital oriented toward the other Se atom. The atomic orbital populations given in Table 10 show that each p orbital on the chalcogen atoms is deficient by about 0.25 e from being completely doubly occupied. The other 0.4 e is split between the two Tl atoms, and there is 0.20 e on each atom, mostly in the "out-of-plane" p orbital with the rest in the p orbital oriented along the Tl−Tl axis. The NBO analysis did not assign any of the orbitals to a weak Tl···Tl or Ch···Ch interaction but to a lone pair. However, this is not inconsistent with the Mayer analysis which looks at the total overlap of the orbitals between atoms. The NBO analysis "assigns" the lone pairs on the Tl atoms to s and p orbitals which can overlap, given the short Tl···Tl distance, thus giving rise to a weak Mayer bond order between the Tl atoms. We note that both analysis methods have some arbitrariness when there are weak interactions, but both show the possibility of a weak Tl···Tl interaction.

The eight highest energy valence MO's for $Tl_2Se_2^{2-}$ are shown in Figure 8 and are similar to those of $Tl_2Te_2^{2-}$. The HOMO (orbital a) is a lone pair ("in-plane" type) on the Se mixed with a lone pair on Tl. The NHOMO (orbital b) is the antibonding combination of the "out-of-plane" lone pairs on the Se atoms. The next highest orbital (orbital c) shows a weak Se···Se interaction with most of the orbital describing lone pairs on Se and Tl. The next highest orbital (orbital d) shows a lone pair type interaction coupled with a bonding orbital between Tl and Se so that the interactions between the two Tl−Se−Tl planes are antibonding. Orbital e is essentially the out-of-plane lone pair on the Se atoms and shows an interaction between the two chalcogens. Orbital f is another mixing of a p orbital lone pair with the Tl−Se bonding orbital. Orbital g shows a Tl···Tl interaction arising mostly from the overlap of the valence s orbitals on the Tl atoms. The most stable orbital is orbital h and is the bonding orbital between the Tl and the Se atoms. The lowest energy valence orbitals (not depicted) are the antibonding (b_1) and bonding (a_1) combinations of the valence s orbitals on the chalcogen.

Three theoretical papers on the electronic structure of the $Tl_2Te_2^{2-}$ anion have been published[17−19] and used geometries constructed from the X-ray structure of $Tl_2Te_2^{2-}$ in (2,2,2-crypt-K^+)$_2Tl_2Te_2^{2-}$·en.[19] Corbett and Burns[19] used simple orbital arguments to rationalize the nonplanarity of the structure. Cave *et al.*[18] used extended Hückel theory and Hartree−Fock calculations with ECP's and a polarized triple ζ valence basis set to calculate the electronic structure of the $Tl_2Te_2^{2-}$ anion and of the tetrahedral-like $Pb_2Sb_2^{2-}$ and $Sn_2Bi_2^{2-}$ anions to determine when a structure is tetrahedral and when it is planar on the basis of electronegativity differences and electron count. They found the butterfly structure of $Tl_2Te_2^{2-}$ to be 48 kcal mol^{-1} more stable than the planar structure. Axe and Marynick[17] used the spin-restricted scattered-wave Xα method to study the $Pb_2Sb_2^{2-}$, $Sn_2Bi_2^{2-}$, and $Tl_2Te_2^{2-}$ anions. They suggest that the simplest

Table 11. Natural Bond Order Analysis for the $Tl_2Ch_2^{2-}$ Anions (Ch = Se and Te)

orbital	orb pop	% s	% p	s (coeff)	p_x (coeff)	p_y (coeff)	p_z (coeff)
				$Tl_2Se_2^{2-}$ [a,b]			
σ(Tl−Se)	1.96 [Tl (16%)]	4.9	94.8	0.18 (−013)	−0.62	0.70 (0.06)	0.25
	[Se (84%)]	11.5	88.5	0.32	0.71	−0.56	−0.27
Tl lp	2.00	93.3	7.7	0.97	−0.24	0.0	−0.08
Tl lp	0.20		99.6		−0.36		0.93
Se lp	1.98	77.4	22.6	0.88		0.47	
Se lp	1.82	2.1	97.8	0.15		−0.36	0.92
				$Tl_2Te_2^{2-}$ [a,c]			
σ(Tl−Te)	1.95 [Tl (17.9%)]	4.93	95.4	−0.16 (013)	−0.61	−0.70 (−0.05)	−0.30
	[Te (82.1%)]	9.5	90.5	0.31	0.71	0.59	0.24
Tl lp	2.00	94.3	5.7	0.97	−0.20		−0.08
Tl lp	0.22		100		−0.44		0.90
Te lp	1.98	79.6	20.4	0.89		0.45	
Te lp	1.81	1.5	98.5	0.15		−0.32	0.94

[a] The symbol lp denotes lone pair. [b] Where Tl−Tl was chosen as the *x* axis, Se−Se was chosen as the *y* axis, and *z* is out of plane. [c] Where Tl−Tl was chosen as the *y* axis, Te−Te was chosen as the *x* axis, and *z* is out of plane.

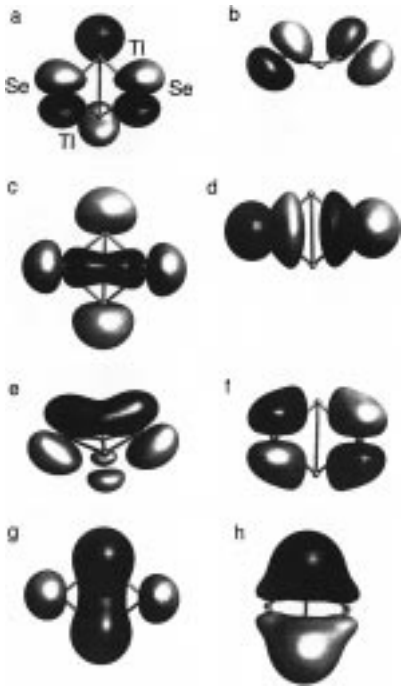

Figure 8. Wave function plots of the upper eight valence molecular orbitals for the $Tl_2Se_2^{2-}$ anion at the NLDFT level and contoured at 0.085. The atom-labeling scheme is given in (a), and the different shades denote two different phases of the orbitals. Key: (a) HOMO (b_1), (b) NHOMO (b_1); (c) third (a_1), (d) fourth (b_1), (e) fifth (a_1), (f) sixth (a_2), (g) seventh (a_1), and (h) eighth (b_2) highest occupied MO. Orbitals (a)−(d) and (h) are responsible for the skeletal bonds in the anions, (e) and (f) are the Se lone pair orbitals, and (g) represents the Tl···Tl interaction arising from overlap of the s orbitals on Tl.

description of the anion is two Te^{2-} anions bonded to two Tl^+ cations and that the difference in the Te···Te and Tl···Tl distances is due to the fact that the Te atoms have larger absolute charges and thus repel each other more than the two Tl atoms. The six highest energy orbitals obtained for the energy-minimized geometries of $Tl_2Se_2^{2-}$ and $Tl_2Te_2^{2-}$ in the present study are similar to those obtained by Axe and Marynick for $Tl_2Te_2^{2-}$ except for orbital c (their $7a_1$) which we show has an overall bonding interaction between the two Te (Se) atoms whereas they ascribe the interaction to donation of the Te atoms to the empty Tl orbitals.

(b) Vibrational Frequencies. The calculated vibrational frequencies are given in Table 6, and the modes for $Tl_2Se_2^{2-}$ and $Tl_2Te_2^{2-}$ are depicted in Figure 6 and are similar for Tl_2SeTe^{2-}, which must be assigned under C_s point symmetry. All of the modes are predicted to be very low in frequency with the highest frequency modes in the range 150−160 cm^{-1} and have been used to assign the experimental spectra (see Raman Spectra of the $Tl_2Ch_2^{2-}$ (Ch = Se, Te) Anions).

The inversion modes in all three anions are predicted to be very low; at the pseudopotential level they are ∼60 cm^{-1} for $Tl_2Se_2^{2-}$, ∼50 cm^{-1} for $Tl_2Te_2^{2-}$, and ∼90 cm^{-1} for Tl_2SeTe^{2-}. The low-frequency values suggest that the potential energy surfaces for inversion of these butterfly-shaped anions are nearly flat and that these anions can be easily distorted along this mode by environmental effects such as crystal packing forces induced by anion···cation interactions or by solvent molecules of crystallization and can easily account for the differences between the fold angles observed for the two experimental structures of $Tl_2Te_2^{2-}$ and those of the calculated gas-phase structures. Although the calculated fold angle of 37° is in better agreement with the value of 39° observed in (2,2,2-crypt-K^+)$_2Tl_2Te_2^{2-}$·en,[19] an even larger discrepancy exists between that of the experimental $Tl_2Se_2^{2-}$ structure (10°) and the calculated value (34°). This coordinate is represented by the lowest energy deformation mode (*vide infra*) and is the most easily deformed and least reliable experimental geometrical parameter for comparison with that of the isolated anion.

(c) Spin−Spin Couplings. The relative magnitudes of the $^2J(^{203}Tl-^{205}Tl)$, $^1J(^{203,205}Tl-^{77}Se)$, and $^1J(^{205}Tl-^{125}Te)$ spin−spin coupling constants may be understood in terms of the calculated s characters of the corresponding bonding interactions. In general, spin−spin couplings between nuclei of heavy atoms connected by single rather than multiple bonds are dominated by the Fermi contact mechanism.[41] In terms of the formalism developed by Pople and Santry,[41] the Fermi contact mechanism is given by eq 1, where all symbols have their usual meanings

$$J_{AB} = 16\frac{\pi^2}{9h}\left(\frac{g\beta h}{2\pi}\right)^2 \gamma_A\gamma_B|\psi_{ns,A}(0)|^2|\psi_{ns,B}(0)|^2\pi_{AB} \qquad (1)$$

and/or values. γ_A and γ_B represent the gyromagnetic ratios of the coupled nuclei, $|\psi_{ns,A}(0)|^2$ and $|\psi_{ns,B}(0)|^2$|are the s-electron densities for the valence *n*s orbitals at nuclei A and B, and π_{AB} is the mutual polarizability of the *n*s orbitals on A and B. In order to make comparisons between couplings in a series of structurally related species having different spin-coupled nuclei, it is necessary to remove the nuclear dependence on J_{AB}. If the Fermi contact mechanism is assumed to be the dominant

(41) Jameson, C. J. In *Multinuclear NMR*; Mason, J., Ed.; Plenum Press: New York, 1987; Chapter 4, p. 89.

contributor to J_{AB}, then the reduced coupling constant, K_{AB},[42] as defined by eq 2, provides a better representation of electronic

$$K_{AB} = \frac{4\pi^2}{h\gamma_A\gamma_B} J_{AB} \quad (2)$$

environments in molecules. Pyykkö and Wiesenfeld[43] have shown that relativistic effects on the s electron density in the Fermi contact term contribute significantly to K_{AB} for heavy main-group elements. Previous work on spin−spin couplings in classically-bonded trigonal-planar $SnCh_3^{2-}$ and $TlCh_3^{3-}$,[20] tetrahedral $SnCh_4^{4-}$,[20] trigonal bipyramidal $Sn_2Ch_3^{2-}$ and $Pb_2Ch_3^{2-}$,[31,32] ditin $Sn_2Ch_6^{4-}$ and $Sn_2Ch_7^{4-}$,[21] and linear $HgCh_2^{2-}$ and $CdCh_2^{2-}$ [20] anions has illustrated a method for factoring out the relativistic effects on the s electron density term, $|\psi_{ns}(0)|^2$. The correction for a given element is determined by applying the ratio $R = |\psi_{ns}(0)|_{rel}^2/|\psi_{ns}(0)|_{nonrel}^2$, where ratios of the relativistic and nonrelativisitic s electron densities are the ratios of the corresponding hyperfine integrals taken from the work of Pyykkö and Wiesenfeld[43] and give the following values: Tl, 3.059; Te, 1.439; Se, 1.155. The relativistically corrected $(K_{Tl-Ch})_{RC}$ and $(K_{Tl-Tl})_{RC}$ values (eq 3) are given in

$$(K_{Tl-Ch})_{RC} = \frac{K_{Tl-Ch}}{R_{Tl}R_{Ch}} \quad (3)$$

Table 4. The one-bond $(K_{Tl-Ch})_{RC}$ couplings are shown to be significantly larger in magnitude than the formal two-bond $(K_{Tl-Tl})_{RC}$ couplings. The Tl−Ch bonds are shown to be predominantly p in character by the orbital population analyses given in Table 9 with much of the s-character isolated on the chalcogen and Tl lone pairs. A relative gauge of the low s-characters in the Tl−Ch bonds of $Tl_2Ch_2^{2-}$ anions is given by the relativistically corrected reduced coupling constants of the trigonal planar $TlSe_3^{3-}$ (15.22×10^{-21} T^2 J^{-1}) and $TlTe_3^{3-}$ (16.36×10^{-21}−16.60×10^{-21} T^2 J^{-1}) anions where the hybridization on Tl is formally sp^2, giving a formal s-character of 33.3% for the Tl−Ch bonds. These couplings are 3.1 and 4.1 times larger than their respective couplings in $Tl_2Se_2^{2-}$ (4.727×10^{-21}−4.752×10^{-21} T^2 J^{-1}) and $Tl_2Te_2^{2-}$ (4.044×10^{-21}−4.060×10^{-21} T^2 J^{-1}). The relative magnitudes of the $(K_{Tl-Ch})_{RC}$ couplings of $TlCh_3^{3-}$ and $Tl_2Ch_2^{2-}$ are consistent with the % s-characters in the Tl−Ch bonds derived from NBO orbital population analysis. The s characters for these bonds are 10.4% for $Tl_2Se_2^{2-}$ and 8.7% for $Tl_2Te_2^{2-}$, and when compared with the formal s-characters of their trigonal planar $TlCh_3^{3-}$ analogs, they are smaller by factors of 3.2 and 3.8, respectively. The ratio of the relativistically corrected reduced coupling constants of the $Tl_2Ch_2^{2-}$ anions, $(K_{Tl-Se})_{RC}/(K_{Tl-Te})_{RC}$ = 1.17, is in good agreement with their relative % s-characters, %s (T1−Se)/%s (Tl−Se) = 1.20, and is also consistent with a Fermi contact dominated mechanism for spin−spin coupling in these anions.

The small Tl···Tl Mayer bond orders (0.14−0.15) are consistent with the smaller $(K_{Tl-Tl})_{RC}$ values when compared to the corresponding $(K_{Tl-Ch})_{RC}$ values (Table 4). Although the NBO analyses do not explicitly assign any of the orbitals to the Tl···Tl interactions in the $Tl_2Ch_2^{2-}$ anions, it is reasonable to expect this interaction to contain a significant s-character on the basis of the high s-orbital character of the Tl lone pairs (Table 11), which are of proper symmetry for overlap. This overlap is represented by orbital g (Figure 8) and shows that the Tl···Tl interaction predominantly arises from overlap of the valence s-orbitals on the Tl atoms.

The Tl−Ch couplings are relatively insensitive to temperature, solvent, and the nature of the countercation; however, the Tl−Tl couplings in all three anions show a high degree of variation when one or all of these parameters are altered (Table 4). The variation of the Tl−Tl coupling is likely associated with the ease with which the fold angle can be deformed by environmental effects such as solvent coordination and is indicated by the low frequencies of the $Tl_2Ch_2^{2-}$ anion inversion modes (Table 6). Variations in the fold angle are expected to have little effect on the magnitudes of ^1J(Tl−Ch) and the Tl−Ch distances, since the Ch atoms are normal to the Tl−Tl fold axis. Moreover, the ease of deformability of the fold angle is supported by the observation of two distinct fold angles and Tl···Tl distances for the $Tl_2Te_2^{2-}$ anion in (2,2,2-crypt-K^+)$_2$-$Tl_2Te_2^{2-}$·en[19] and in (2,2,2-crypt-K^+)$_2Tl_2Te_2^{2-}$ (this work) and by the calculated optimized geometries of the $Tl_2Te_2^{2-}$ and $Tl_2Se_2^{2-}$ anions which give fold angles that differ significantly from those observed in the experimental structures.

Conclusion

The solution structures of the natural abundance $Tl_2Ch_2^{2-}$ (Ch = Se and/or Te) and the ^{77}Se isotopically enriched $Tl_2Se_2^{2-}$ anions have been studied by variable-temperature multi-NMR spectroscopy and confirmed by a detailed analysis of the first-order ^{203}Tl, ^{205}Tl, and ^{77}Se subspectra arising from natural abundance and ^{77}Se-enriched isotopomer distributions. The X-ray crystal structure of the $Tl_2Se_2^{2-}$ anion has been determined for the first time and that of $Tl_2Te_2^{2-}$ has been determined in the absence of solvent in the crystal lattice. Density functional theory calculations confirmed that the butterfly geometries observed for the $Tl_2Ch_2^{2-}$ anions in the solid state are true minima in the gas phase but are highly deformable about the fold angle and are supported by the observed variation in the Tl−Tl coupling constants with solvent and temperature and by the observed and calculated low frequencies of the anion inversion modes. The present $Tl_2Te_2^{2-}$ anion structure was also shown by DFT calculations to be a better approximation of the gas-phase geometry than that reported in (2,2,2-crypt-K^+)$_2Tl_2$-Te_2^{2-}·en.[19] The magnitudes of the $(K_{Tl-Ch})_{RC}$ and $(K_{Tl-Tl})_{RC}$ coupling constants were shown to correlate with the calculated % s-characters determined for the corresponding bonds. Theory indicates that the Tl−Ch bonds are 2-center−2-electron bonds of high p-character and that there is a significant concentration of s-electron density between the Tl atoms corresponding to bond orders of 0.14-0.15.

Experimental Section

Apparatus and Materials. All compounds employed are air sensitive. Consequently, all manipulations were performed under rigorously anhydrous conditions and in the absence of oxygen in a two-station nitrogen-atmosphere drybox (Vacuum Atmospheres Model DLX, with moisture and oxygen levels < 0.1 ppm; for general solid and crystal handling), on a general-purpose grease-free glass vacuum line equipped with glass/FEP stopcocks (J. Young Scientific Glassware), or in a glovebag (for solution handling) which had been purged with dry nitrogen for at least 12 h prior to use.

Potassium (BDH Chemicals, >99%) and sodium (BDH Chemicals, >99.8%) were cleaned as previously described,[35] and freshly cut samples were handled only in the drybox. Thallium rod (Alfa Inorganics, 99%), tellurium powder (Alfa Inorganics, 99.5%), selenium shot (Alfa Inorganics, 99.9%), 94.4% ^{77}Se-enriched selenium (Technabsexport, Moscow, Russia), and 2,2,2-crypt 1,10-diaza(4,7,13,16,21,-24-hexaoxabicyclo[8.8.8]hexacosane; Merck, 99%) were dried in the

(42) Pople, J. A.; Santry, D. P. *Mol. Phys.* **1964**, *8*, 1.
(43) Pyykkö, P.; Wiesenfeld, L. *Mol. Phys.* **1981**, *43*, 557.

evacuated port of the drybox for a minimum of 45 min followed by exposure to the atmosphere of the drybox for at least 2 days prior to use. The oxide layer on the thallium rod was shaved off with a scalpel inside the drybox prior to use.

All solvents were thoroughly dried, transferred by vacuum distillation, and stored in round-bottom flasks equipped with glass/Teflon stopcocks. Tetrahydrofuran (Aldrich, 99.9%) was stored over freshly cut sodium wire (BDH Chemicals, 99.8%). Ethylenediamine (Fisher Scientific Co., 99%) and ethylamine (Aldrich, 99%) were dried over CaH_2 powder (BDH Chemicals) for several weeks and then vacuum distilled onto, and stored over, fresh CaH_2 for at least 1 additional week prior to use. Anhydrous ammonia (Matheson) was further dried over freshly cut sodium metal at −78 °C for at least 1 week prior to use.

Preparation of the Alloys. The Tl_2Te, MTlCh (M = Na, K; Ch = Se, Te), and $KTlSe_{0.5}Te_{0.5}$ alloys were prepared as previously described[20] by fusion of the elements in the required molar ratios inside thick-walled Pyrex tubes. The 94.4% ^{77}Se-enriched KTlSe alloy (hereafter referred to as KTl^{77}Se) was prepared in two steps involving the fusion of KTl in a Pyrex tube followed by fusion with enriched ^{77}Se in a quartz vessel. The following amounts were used. Tl_2Te: Tl, 3.9496 g, 19.33 mmol; Te, 1.2231 g, 9.59 mmol. KTlSe: K, 1.1424 g, 29.22 mmol; Tl, 5.9765 g, 29.24 mmol; Se, 2.2973 g, 29.04 mmol. $KTlSe_{0.5}Te_{0.5}$: K, 1.2927 g, 33.06 mmol; Tl, 6.2140 g, 30.41 mmol; Se, 1.1841 g, 15.00 mmol; Te, 1.9712 g, 15.45 mmol. KTlTe: K, 0.9467 g, 24.21 mmol; Tl, 4.9496 g, 24.22 mmol; Te, 3.1034 g, 24.32 mmol. NaTlTe: Na, 0.2202 g, 9.58 mmol; Tl, 1.9069 g, 9.331 mmol; Te, 1.2423 g, 9.74 mmol. KTl^{77}Se: KTl, 0.0803 g, 0.33 mmol; Se, 0.0261 g, 0.33 mmol. The resulting alloys were ground into fine powders. Potassium monotelluride, K_2Te, was prepared as previously described.[20]

Preparation of the $Tl_2Ch_2^{2-}$ (Ch = Se and/or Te) Solutions for NMR Spectroscopy. The anions were prepared by extracting the MTlCh and $KTlSe_{0.5}Te_{0.5}$ alloys in en or liquid NH_3 in the presence of a 10−40 mol % excess of 2,2,2-crypt with respect to M^+. The resulting solutions were isolated for NMR spectroscopy as previously described.[20] The following quantities of reagents were used to prepare the alloy extracts with values for the 94.4% ^{77}Se-enriched $Tl_2Se_2^{2-}$ anion given in brackets: $Tl_2Se_2^{2-}$ in NH_3 (KTlSe, 0.1190 [0.1064] g, 0.369 [0.330] mmol; 2,2,2-crypt, 0.1894 [0.1474] g, 0.503 [0.391] mmol); $Tl_2Se_2^{2-}$ and Tl_2SeTe^{2-} in en ($KTlSe_{0.5}Te_{0.5}$, 0.1323 g, 0.382 mmol; 2,2,2-crypt, 0.1670 g, 0.444 mmol); $Tl_2Se_2^{2-}$ and Tl_2SeTe^{2-} in NH_3 ($KTlSe_{0.5}Te_{0.5}$, 0.1571 g, 0.453 mmol; 2,2,2-crypt, 0.1794 g, 0.476 mmol); $Tl_2Te_2^{2-}$ in en (NaTlTe, 0.1027 g, 0.289 mmol; 2,2,2-crypt, 0.1143 g, 0.304 mmol); $Tl_2Te_2^{2-}$ in NH_3 (KTlTe, 0.1094 g, 0.295 mmol; 2,2,2-crypt, 0.1193 g, 0.317 mmol).

Crystal Growing. (a) (2,2,2-crypt-K^+)$_2Tl_2Se_2^{2-}$. The natural abundance KTlSe alloy (0.1012 g, 0.314 mmol) was transferred into one arm of a two-arm Pyrex vessel and extracted in en in the presence of a 23 mol % excess of 2,2,2-crypt (0.1453 g, 0.386 mmol) with respect to K^+. After 1 week, the resulting red solution was decanted into the second arm of the vessel. A slight excess of THF (v/v) was condensed under static vacuum at 0 °C into the first arm of the Pyrex reactor. The reactor was allowed to stand for 2-3 weeks over which time the THF slowly vapor-phase diffused into the en solution, resulting in the formation of dark red cubic crystals and red plates. The mother liquor was decanted back into the first arm of the Pyrex vessel and slowly pumped off under static vacuum into a previously vacuum-dried Pyrex vessel which was initially held at −78 °C and then cooled to −196 °C. The crystalline sample was dried under dynamic vacuum at room temperature and transferred to a drybox equipped with a stereomicroscope. Suitable crystals were cut and then heat sealed inside 0.5 mm Lindemann glass capillaries.

(b) (2,2,2-crypt-K^+)$_2Tl_2Te_2^{2-}$. All attempts to prepare suitable single crystals of $Tl_2Te_2^{2-}$ from en extracts of the NaTlTe alloy in the presence of a 20 mol % excess of 2,2,2-crypt (with respect to Na^+) gave rise to microcrystalline material. The dark red solution resulting from the reaction of K_2Te (0.0886 g, 0.430 mmol) and Tl_2Te (0.1124 g, 0.209 mmol) in a en/ethylamine (1:1 v/v) mixture in the presence of a 37 mol % deficit of 2,2,2-crypt (0.2032 g, 0.540 mmol) with respect to K^+ was shown by ^{203,205}Tl NMR spectroscopy to contain $Tl_2Te_2^{2-}$. This solution was transferred into one arm of a two-arm Pyrex vessel under the dry nitrogen atmosphere of a glovebag. Vapor-phase diffusion of THF into the red solution over a period of 3 d led to the formation of deep-red hexagonal plates. The mother liquor was decanted back into the first arm of the Pyrex vessel and removed under the dry nitrogen atmosphere of a glovebag. The crystalline sample was dried under dynamic vacuum at room temperature and transferred to the drybox. Suitable crystals were mounted inside 0.5 mm Lindemann glass capillaries and heat sealed.

Collection and Reduction of X-ray Data. The crystals used for data collection had the following dimensions: $0.35 \times 0.41 \times 0.48$ mm^3 [(2,2,2-crypt-K^+)$_2Tl_2Se_2^{2-}$] and $0.45 \times 0.12 \times 0.28$ mm^3 [(2,2,2-crypt-K^+)$_2Tl_2Te_2^{2-}$].

(a) (2,2,2-crypt-K^+)$_2Tl_2Se_2^{2-}$. A suitable crystal was centered on a four-circle Syntex P3 diffractometer, using silver radiation monochromatized with a graphite crystal (λ = 0.560 86 Å). Unit cell dimensions were determined at 24 °C from a least-squares refinement of the setting angles (χ, ϕ, and 2θ) obtained from 29 accurately centered reflections (with $14.87 \le 2\theta \le 24.39°$) chosen from a variety of points in reciprocal space. Their peak profiles revealed a single crystal. Integrated diffraction intensities were collected using an ω-scan technique with scan rates varying from 1.5 to 14.6° min^{-1} and a scan range of ±0.5° so that weaker reflections were examined more slowly to minimize counting errors. Data were collected with $0 \le h \le 12$, $0 \le k \le 11$, and $-23 \le l \le 23$ and with $4 \le 2\theta \le 35°$. During data collection, the intensities of three standard reflections were monitored every 97 reflections to check for crystal stability and alignment. No crystal decay was observed. A total of 3724 reflections were measured of which 3523 were independent and were used for structure solution. Corrections were made for Lorentz and polarization effects. Absorption corrections were not applied.

(b) (2,2,2-crypt-K^+)$_2Tl_2Te_2^{2-}$. Crystal data on a single crystal were collected on a Stoe imaging plate diffractometer system equipped with a one-circle goniometer and a graphite monochromator. Molybdenum radiation (λ = 0.710 73 Å) was used. Unit cell dimensions were obtained from 1339 accurately centered reflections (with $3 \le 2\theta \le 29°$). Integrated diffraction intensities were obtained at two crystal-to-detector distances by using oscillation scans with $-15 \le h \le 15$, $-15 \le k \le 15$, and $-16 \le l \le 16$ and with $3 \le 2\theta \le 29°$: (a) 400 exposures (5 min per exposure) at 50 mm with $80 \le \phi \le 280°$ and with the crystal oscillated 0.5° in ϕ; (b) 200 exposures (1.5 min per exposure) at 125 mm with $0 \le \phi \le 240°$ and with the crystal oscillated through 1.2° in ϕ. The two data sets were merged, and the final data set contained 92% of the calculated number of unique reflections. A total of 16 178 reflections were measured, and 6155 remained after averaging of equivalent reflections. Corrections were made for Lorentz and polarization effects, and absorption correction were not applied.

Solution and Refinement of the Structures. All calculations were performed on a Silicon Graphics, Inc., model 4600PC workstation using the SHELXTL-Plus package[44] for structure determination, refinement, and molecular graphics.

The XPREP program[44] was used to confirm the unit cell dimensions and the crystal lattices. The solution was obtained using conventional direct methods which located the general and/or special positions of the main group and alkali metal atoms, revealing that the $Tl_2Te_2^{2-}$ anion was disordered about a center of symmetry. The full-matrix least-squares refinement of the positions and isotropic thermal parameters of the assigned atoms located the general and/or special positions of the C, N, and O atoms of the 2,2,2-crypt-K^+ cations. In the case of $Tl_2Se_2^{2-}$, the location of the K atoms of the 2,2,2-crypt-K^+ on *.m.* implied a positional disorder for the cations. Hydrogen atom positions were calculated [d(C−H) = 0.96 Å; U(H) fixed to $-1.2U$(C)]. During the final stages of the refinement, 11 [(2,2,2-crypt-K^+)$_2Tl_2Se_2^{2-}$] and 44 [(2,2,2-crypt-K^+)$_2Tl_2Te_2^{2-}$] reflections with $F_o^2 < -2\sigma(F_o^2)$ were suppressed for potential systematic errors and weighting factors recommended by the refinement program were introduced. The maximum electron densities in the final difference Fourier maps were located around the anions.

Multinuclear Magnetic Resonance Spectroscopy. The ^{203}Tl, ^{205}Tl, and ^{77}Se NMR spectra were recorded on a Bruker AC-200 (4.698

(44) Sheldrick, G. M. *SHELXTL-Plus*, Release 5.03. Siemens Analytical X-ray Instruments, Inc.: Madison, WI, 1994.

T) pulse spectrometer by inserting a 10-mm Bruker AC-300 broad band probe (13.968−121.497 MHz) into the AC-200 cryomagnet. Spectra were routinely obtained without locking (field drift < 0.1 Hz h^{-1}). The observed spectrometer frequencies were 38.168 (^{77}Se), 114.320 (^{203}Tl), and 115.447 (^{205}Tl) MHz. Free-induction decays were typically accumulated in 16 or 32 K of memory. Spectral width settings of 25−100 kHz were employed, yielding data point resolutions of 3.05−6.10 Hz/data point and acquisition times of 0.328−0.164 s, respectively. Relaxation delays were not applied. Typically, 10 000−100 000 transients were accumulated depending on the concentrations and sensitivities of the nuclides under study. Pulse-width settings corresponding to a bulk magnetization tip angle, θ, of ∼90° were 12.0 (^{77}Se), 20.0 (^{203}Tl), and 10.0 (^{205}Tl) μs. Line broadening parameters used in the exponential multiplication of the free induction decays were 10−20 Hz for narrow lines and 100 Hz for broad lines. Variable-temperature spectra were recorded using the variable-temperature controllers of the spectrometers, and temperatures (accurate to ±1.0 °C and stable to within ±0.10 °C) were checked by placing a copper−constantan thermocouple in the sample region of the probe. Samples were allowed to equilibrate for at least 5 min while spinning before spectral accumulations were begun.

The ^{77}Se, ^{203}Tl, and ^{205}Tl chemical shifts were referenced externally to neat samples of $(CH_3)_2Se$ and 0.1 M aqueous $TlNO_3$ at 24 °C. The chemical shift convention used was a positive (negative) sign signifies a chemical shift to high (low) frequency of the reference compound.

The ^{203}Tl and ^{205}Tl NMR subspectra of the $Tl_2Ch_2^{2-}$ were simulated and summed by using the program DSYMPC.[45] Subspectra were weighted by using the normalized total line intensities listed in Table 5 and summed by using the line spectrum addition subroutine in DSYMPC.

Raman Spectroscopy. Raman spectra were recorded on a Bruker Equinox 55 FT-IR spectrometer equipped with an FRA 106/S FT-Raman accessory which employed a CaF_2 beamsplitter and a liquid-nitrogen-cooled Ge diode detector. The backscattered (180 °C) radiation was sampled. Rayleigh filters consisting of a series of transmission and reflection filters were used. The scanner velocity was 50 kHz and the wavelength range for acquisition was 5500−10 500 cm^{-1} when shifted relative to the laser line at 9394 cm^{-1}, giving a spectral range of 3895 to −1105 cm^{-1}. The actual usable Stokes range was 50−3500 cm^{-1} with a spectral resolution of 4 cm^{-1}. The Fourier transformations were carried out by using a Blackman Harris 3-term apodization and a zero-filling factor of 2. The 1064-nm line of a Nd YAG laser (350 mW maximum output) was used for excitation of the samples with a laser spot of *ca*. 0.2 mm. The spectra were recorded at room temperature by using laser powers of 40 mW for (2,2,2-crypt-$K^+)_2Tl_2Se_2^{2-}$ and 70 mW for (2,2,2-crypt-$K^+)_2Tl_2Te_2^{2-}$ and were corrected for instrument response. The powdered samples were loaded into Pyrex melting point capillaries inside a drybox; the capillaries had been dried at 250 °C under vacuum for at least 1 day.

Calculations. The initial calculations were performed with the density functional theory (DFT) program DGauss[46] on Silicon Graphics, Inc., computers at the local (LDFT) and nonlocal (NLDFT, gradient-corrected) levels. Calculations were performed with a basis set in which the Tl core electrons were treated with a pseudopotential (PP),[47] and the remaining electrons were treated with a polarized valence double ζ basis set. For the Se and Te atoms, calculations were performed with the same type of pseudopotential and valence basis set as those used for Tl as well as with all-electron, polarized valence double ζ (DZVP) basis sets.[48] All-electron DZVP basis set calculations were also performed on the isoelectronic $In_2Se_2^{2-}$ and $In_2Te_2^{2-}$ anions for comparison. The local potential fit of Vosko, Wilk, and Nusair[49] was used (VWN/PP/PP and VWN/PP/DZVP). The gradient-corrected (nonlocal) density functional calculations were done with the nonlocal exchange potential of Becke[50] together with the nonlocal correlation function of Perdew (BP/PP/PP and BP/PP/DZVP).[51] In order to check the dependence of the calculated results on the form of the treatment of the core electrons, additional calculations were carried out by using the effective core potentials (ECP) and the basis sets of Stevens *et al.*[52] The ECP for Tl has the 4d and 4f electrons in the core and the 5s, 5p, and 5d electrons in the valence space. For Se and Te, only the *n*s and *n*p (n = 4 for Se and 5 for Te) electrons are in the valence space. The d polarization functions were taken from Huzinaga's compilation.[53] The calculations were performed at the local level with the program Gaussian 94.[54]

The geometries were optimized by using analytic gradient methods. Second derivatives were calculated by numerical differentiation of the analytic first derivatives except for the all-electron calculations on the $In_2Ch_2^{2-}$ anions where analytic methods were used.[55] For the finite difference calculations, a two-point method with a finite difference of 0.01 au was used. Bond orders and valencies were calculated by following the method of Mayer.[39]

Acknowledgment. We thank the Natural Sciences and Engineering Research Council (NSERC) of Canada for support in the form of a research grant. We also thank NSERC and the Ontario Ministry of Education and Training for the award of graduate scholarships to J.C. and A.M.P., respectively. We gratefully acknowledge Prof. Dr. Arndt Simon, Max-Planck-Institut, Stuttgart, Germany, for making the Stoe imaging plate diffractometer system available and Janice Hellman, Bruker Spectrospin, Milton, Ontario, Canada, for recording the Raman spectra. The density functional theory calculations were performed under the auspices of the Office of Basic Energy Sciences, U.S. Department of Energy, under Contract DE-AC06-76RLO 1830 with the Battelle Memorial Institute, which operates the Pacific Northwest National Laboratory, a multiprogram national laboratory operated from the Department of Energy.

Supporting Information Available: Crystal data and structure refinement parameters (Table S1), atomic coordinates and equivalent isotropic displacement parameters for the 2,2,2-crypt-K^+ cations (Table S2), bond lengths and bond angles in the 2,2,2-crypt-K^+ cations (Table S3), anisotropic displacement parameters (Table S4), and atomic coordinates and *U* values for the hydrogen atoms (Table S5) (18 pages). Ordering information is given on any current masthead page.

IC9710465

(45) Hägele, G.; Höffken, H.-W.; Mistry, F.; Spiske, R.; Weber, U.; Goudetsidis, S. *DSYMPC*, release 0.940728E; Institut für Anorganische Chemie und Strukturchemie, Heinrich-Heine-Universität: Düsseldorf, Germany, 1994.

(46) (a) Andzelm, J.; Wimmer, E.; Salahub, D. R. In *The Challenge of d and f Electrons: Theory and Computation*; Salahub, D. R., Zerner, M. C., Eds.; ACS Symposium Series, No. 394; American Chemical Society: Washington, DC, 1989; p 228. (b) Andzelm, J. In *Density Functional Theory in Chemistry*; Labanowski, J., Andzelm, J., Eds.; Springer-Verlag: New York, 1991; p 155. (c) Andzelm, J.; Wimmer, E. *J. Chem. Phys.* **1992**, *96*, 1280.

(47) Chen, H.; Kraskowski, M.; Fitzgerald, G. *J. Chem. Phys.* **1993**, *98*, 8710. (b) Troullier, N.; Martins, J. L. *Phys. Rev. B* **1991**, *43*, 1993.

(48) Godbout, N.; Salahub, D. R.; Andzelm, J.; Wimmer, E. *Can. J. Chem.* **1992**, *70*, 560.

(49) Vosko, S. J.; Wilk, L.; Nusair, W. *Can. J. Phys.* **1980**, *58*, 1200.

(50) (a) Becke, A. D. *Phys. Rev. A* **1988**, *38*, 3098. (b) Becke, A. D. In *The Challenge of d and f Electrons: Theory and Computation*; Salahub, D. R., Zerner, M. C., Eds.; ACS Symposium Series, No. 394; American Chemical Society: Washington, DC, 1989; p 166. (c) Becke, A. D. *Int. J. Quantum. Chem. Symp.* 1989, *23*, 599.

(51) Perdew, J. P. *Phys. Rev. B* **1986**, *33*, 8822.

(52) Stevens, W. J.; Krauss, M.; Basch, H.; Jasien, P. G. *Can. J. Chem.* **1992**, *70*, 216.

(53) Huzinaga, S.; Andzelm, J.; Klobukowski, M.; Radzio-Andzelm, E.; Sakai, Y.; Tatewaki, H. *Gaussian Basis Sets for Molecular Calculations*; Physical Sciences Data 16; Elsevier: Amsterdam, 1984.

(54) Frisch, M. J.; Trucks, G. W.; Schlegel, H. B.; Gill, P. M. W.; Johnson, B. G.; Robb, M. A.; Cheeseman, J. R.; Keith, T. A.; Peterson, G. A.; Montgomery, J. A.; Raghavachari, K.; Al-Laham, M. A.; Zakrzewski, V. G.; Ortiz, J. V.; Foresman, J. B.; Cioslowski, J.; Stefanov, B. B.; Nanayakkara, A.; Challacombe, M.; Peng, C. Y.; Ayala, P. Y.; Chen, W.; Wong, M. W.; Andres, J. L.; Replogle, E. S.; Gomperts, R.; Martin, R. L.; Fox, D. J.; Binkley, J. S.; Defrees, D. J.; Baker, J.; Stewart, J. J. P.; Head-Gordon, M.; Gonzalez, C.; Pople, J. A. *Gaussian 94*; Gaussian, Inc.: Pittsburgh, PA, 1995.

(55) Komomicki, A.; Fitzgerald, G. *J. Phys. Chem.* **1993**, *98*, 1398 and references therein.